

# Trench migration and overriding plate stress in dynamic subduction models

A. F. Holt,<sup>1</sup> T. W. Becker<sup>1</sup> and B. A. Buffett<sup>2</sup>

<sup>1</sup>Department of Earth Sciences, University of Southern California, 3651 Trousdale Parkway, Los Angeles, CA 90089, USA. E-mail: adamholt@usc.edu

<sup>2</sup>Department of Earth and Planetary Science, University of California, Berkeley, CA 94720, USA

Accepted 2015 January 6. Received 2014 November 7; in original form 2014 June 25

## SUMMARY

On Earth, oceanic plates subduct beneath a variety of overriding plate (OP) styles, from relatively thin and negatively buoyant oceanic OPs to thick and neutrally/positively buoyant continental OPs. The inclusion of an OP in numerical models of self-consistent subduction has been shown to reduce the rate that subducting slabs roll back relative to the equivalent single plate models. We use dynamic, 2-D subduction models to investigate how the mechanical properties, namely viscosity, thickness, and density, of the OP modify the slab rollback rate and the state of stress of the OP. In addition, we examine the role of the subducting plate (SP) viscosity. Because OP deformation accommodates the difference between the slab rollback rate and the far-field OP velocity, we find that the temporal variations in the rollback rate results in temporal variations in OP stress. The slabs in our models roll back rapidly until they reach the lower mantle viscosity increase, at which point the rollback velocity decreases. Concurrent with this reduction in rollback rate is a switch from an OP dominated by extensional stresses to a compressional OP. As in single plate models, the viscosity of the SP exerts a strong control on subducting slab kinematics; weaker slabs exhibit elevated sinking velocities and rollback rates. The SP viscosity also exerts a strong control on the OP stress regime. Weak slabs, either due to reduced bulk viscosity or stress-dependent weakening, have compressional OPs, while strong slabs have dominantly extensional OPs. While varying the viscosity of the OP alone does not substantially affect the OP stress state, we find that the OP thickness and buoyancy plays a substantial role in dictating the rate of slab rollback and OP stress state. Models with thick and/or negatively buoyant OPs have reduced rollback rates, and increased slab dip angles, relative to slabs with thin and/or positively buoyant OPs. Such elevated trench rollback for models with positively buoyant OPs induces extensional stresses in the OP, while OPs that are strongly negatively buoyant are under compression. While rollback is driven by the negative buoyancy of the subducting slab in such models of free subduction, we conclude that the physical properties of the OP potentially play a significant role in modulating both rollback rates and OP deformation style on Earth.

**Key words:** Mantle processes; Creep and deformation; Subduction zone processes; Backarc basin processes; Dynamics of lithosphere and mantle; Rheology: crust and lithosphere.

## 1 INTRODUCTION

The subduction of a negatively buoyant lithospheric plate below an overriding plate (OP) and into the sublithospheric mantle is one of the fundamental components of plate tectonics and yet the degree of control that the mechanical properties of the OP have on the dynamics of the subducting plate (SP) is not entirely clear. Subduction of oceanic plates of various ages occurs beneath OPs with a broad range of mechanical properties, with continental OPs typically thicker and more positively buoyant than their oceanic counterparts. Tomographic images of subduction zones show that

slabs subduct with a wide range of upper-mantle dip angles and exhibit a wide variety of deformation styles upon reaching the transition zone, from slabs that appear to flatten or fold (e.g. Japan) to slabs that appear to extend deep into the lower mantle with a wide variety of dip angles (e.g. Central America) (e.g. Li *et al.* 2008). Dynamic modelling studies that consider the SP in isolation show that the viscosity of the subducting slab, relative to that of the surrounding mantle, exerts a strong control on slab evolution, particularly the rate at which the slab hinge rolls back (e.g. Fumicello *et al.* 2003; Schellart 2004; Bellahsen *et al.* 2005; Enns *et al.* 2005; Stegman *et al.* 2006; Di Giuseppe *et al.* 2008; Ribe 2010). The

rollback rate significantly affects subducting slab morphology, with slabs that rapidly roll back typically having reduced dips (Uyeda & Kanamori 1979; Garfunkel *et al.* 1986; Kincaid & Olson 1987; Griffiths *et al.* 1995; Christensen 1996). If subducting slabs have sufficiently low viscosity and density, such reduced dips result in an elevated propensity for slab flattening in the transition zone (e.g. Davies 1995; Christensen 1996; Čížková *et al.* 2002; Enns *et al.* 2005; Ribe 2010). While rollback is driven by the negative buoyancy of the subducting slab in free subduction models, it has been shown that the presence of an OP significantly reduces slab rollback velocities (e.g. Yamato *et al.* 2009; Butterworth *et al.* 2012). Motivated by the wide range of OPs present on Earth, we investigate the degree to which variable OP properties (density, thickness and viscosity) can contribute to explaining the wide range of rollback rates, and slabs dips, observed.

In single plate models, relatively high viscosity slabs exhibit elevated rollback, lower viscosity slabs have near-stationary trenches, and intermediate viscosity slabs (factor  $\sim 100$ –10 000 more viscous than mantle), such as those modelled here, exhibit a wide range of rollback styles/rates (e.g. Funiciello *et al.* 2003, 2008; Schellart 2004; Bellahsen *et al.* 2005; Enns *et al.* 2005; Stegman *et al.* 2006; Faccenna *et al.* 2007; Di Giuseppe *et al.* 2008; Ribe 2010). The dip of the subducting slab as it impinges on the base of the model domain or a viscosity discontinuity, which is related to the amount of rollback that has occurred, is then thought to dictate the subsequent style of slab evolution (Di Giuseppe *et al.* 2008; Schellart 2008b; Ribe 2010). In addition to explicitly examining the how the OP mechanical properties affect subduction dynamics, we investigate how lithospheric viscosity affects subduction dynamics in two-plate models, thereby taking into account the viscosity of both the SP and OP.

After examining subducting slab dynamics for uniformly strong (factor 2000 plate-mantle viscosity contrast) and weak (factor 100 viscosity contrast) lithospheric plates, we investigate the role of stress-dependent viscosities. Laboratory experiments predict that deformation in high stress regions is dominated by dislocation creep, in which the effective viscosity has a power-law dependence on stress (e.g. Karato & Wu 1993; Hirth & Kohlstedt 2003). Models that do include an OP, yet restrict trench motion, show that the inclusion of a stress-dependent rheology decreases the viscosity of the mantle wedge which reduces hydrodynamic stresses on the upper surface of the slab, and so increases the dip angle (Billen & Hirth 2005, 2007). Additionally, the inclusion of pseudo-plastic behaviour, with a yield stress that is sufficiently low to weaken the portion of the slab that bends at the 660 km viscosity jump, has been shown to prohibit the penetration of a slab into the lower mantle (Čížková *et al.* 2002, 2007; Čížková & Bina 2013). Because we allow the trench to migrate freely, this study allows the stress-dependent rheology to exert a control on trench migration, and so the migration-related component of slab dip.

The inclusion of an OP, coupled to the SP by a weak crust and mantle flow tractions, enables an investigation into how the lithospheric properties affect the stresses induced in the OP by subduction (e.g. Clark *et al.* 2008; Capitanio *et al.* 2010a, 2011; Schellart & Moresi 2013). On Earth, large scale OP deformation of the OP ranges from the compressional ‘Chilean type’ to the extensional ‘Marianas type’ (Uyeda & Kanamori 1979). A link between the OP stress regime and slab rollback has been suggested based on kinematic constraints, in that OP deformation must accommodate the disparity between rollback and far-field OP motion (e.g. Jarrard 1986). OP extension is expected in the case of purely slab-buoyancy driven trench retreat with a passive OP (e.g. Elsasser

1971; Molnar & Atwater 1978; Schellart 2008a), whereas a component of OP compression is expected where the OP is driving, or at least contributing to, the trench retreat (e.g. Jarrard 1986; Heuret & Lallemand 2005; Heuret *et al.* 2007). Because there are exceptions to both end-members on Earth, it appears that the complexity of subduction zones prohibits such a single overarching mechanism for large scale subduction-induced OP deformation (e.g. Carlson & Melia 1984; Sdrolias & Müller 2006; Schellart 2008a). Even in free subduction models, in which the OP is not externally pushed towards the SP, near-trench OP compression is observed (Capitanio *et al.* 2010a, 2011; Schellart & Moresi 2013). This is due to subduction-induced flow in the mantle wedge, and suggests a departure from either the slab-driven or OP-driven idealized models, even when far-field forcing effects are neglected. We examine how lithospheric rheology and OP mechanical properties can, even in the absence of external forces, influence the slab-driven OP stress regime, and contribute to the generation of the range of OP deformation regimes observed on Earth.

We investigate the controls on subducting slab evolution, and OP stress, using fully dynamic, 2-D subduction models. Time-progressive numerical modelling studies of subduction with an OP often kinematically constrain the subducting slab by imposing plate/mantle velocities (e.g. van Hunen *et al.* 2000; Čížková *et al.* 2002; Billen & Hirth 2005; van Dinther *et al.* 2010; Ghazian & Buiter 2013) and/or fix the position or shape of the weak zone/fault which decouples the two plates (e.g. Gurnis & Hager 1988; King & Hager 1994; Čížková *et al.* 2002; Běhouková & Čížková 2008; van Hunen & Allen 2011; Bottrill *et al.* 2012). Fixing the trench position inhibits slab rollback/advance and so places a non-physical constraint on the evolution of the slab, and prescribing a surface velocity can add artificial energy to the system if the imposed velocity/viscosity is not consistent with that derived from the purely buoyancy-driven problem (Han & Gurnis 1999). This study aims to improve our understanding of the role of the OP using numerical models in which flow is driven entirely by buoyancy forces. The free-trench models of Zhong & Gurnis (1995) demonstrate that the rate of trench rollback decreases as slabs penetrate into the lower mantle, and the dynamic models of Sharples *et al.* (2014) show that slabs with thicker OPs resist trench retreat more than those with thin OPs. Recent work by Garel *et al.* (2014) shows that, using dynamic two-plate thermomechanical models, the wide range of slab morphologies observed on Earth can be reproduced with various SP-OP age combinations and a upper-lower mantle viscosity increase of factor 30. We use a simplified rheological setup relative to Garel *et al.* (2014) and, instead of testing the role of SP/OP plate age (i.e. all mechanical properties dictated by age-dependent thermal structure), we vary the lithospheric viscosity, thickness, and density of the OP individually, in order to illuminate the various mechanisms potentially operating on Earth.

## 2 MODEL DESCRIPTION

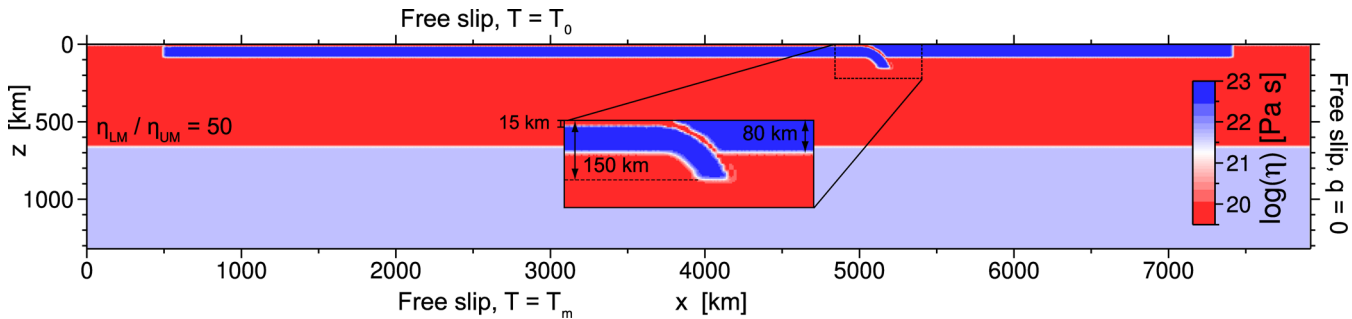
### 2.1 Numerical method and model setup

We use the finite-element code CitcomCU to solve the equations governing convection in an incompressible (Boussinesq approximation), viscous fluid with negligible inertia and, in our case, zero internal heating (e.g. Moresi & Gurnis 1996; Zhong 2006). The equations solved—the conservation of mass, momentum and energy—are given in non-dimensional form below:

$$\nabla \cdot \mathbf{u} = 0 \quad (1)$$

**Table 1.** Model parameters.

Symbol	Parameter	Reference (range)	Units
$h_l$	Lithospheric thickness	80 (40–120)	km
$h_c$	Crustal thickness	15	km
$w_u$	Overriding plate length	2200	km
$w_s$	Subducting plate length	4750	km
$h$	Domain height	1320	km
$w$	Domain width	7920	km
$T_0$	Surface/lithospheric temperature	273	K
$T_m$	Mantle temperature	1573	K
$\rho_0$	Reference density	3300	$\text{kg m}^{-3}$
$\alpha$	Thermal expansivity	$1.5 \times 10^{-5}$	$\text{K}^{-1}$
$\kappa$	Thermal diffusivity	$10^{-6}$	$\text{m}^2 \text{s}^{-1}$
$\eta_0(\eta_{\text{mant}})$	Reference/mantle viscosity	$10^{20}$	$\text{Pa s}$
$\eta_c$	Crust viscosity	$2 \times 10^{19}$	$\text{Pa s}$
$E$	Frank-Kamenetskii parameter	6.21 (4.61–7.60)	—
$n$	Power-law exponent	1 (1, 3.5)	—
$\sigma_T$	Power-law transition stress	100 (50–150)	MPa
$b$	Byerlee cohesion	60	MPa
$a$	Byerlee friction coefficient	0.6	—
$\lambda$	Byerlee pore pressure factor	0.15	—

**Figure 1.** Initial viscosity field for the reference model (see Table 1 for reference parameters).

$$\nabla p + \nabla \cdot [\eta(\nabla \mathbf{u} + \nabla \mathbf{u}^T)] + Ra T \mathbf{e}_z = 0 \quad (2)$$

$$\frac{\partial T}{\partial t} + \mathbf{u} \cdot \nabla T = \nabla^2 T \quad (3)$$

where  $\mathbf{u}$  is velocity,  $p$  is dynamic pressure,  $\eta$  is viscosity,  $T$  is temperature,  $\mathbf{e}_z$  is a unit vector in the vertical direction and  $Ra$  is the Rayleigh number given by:

$$Ra = \frac{\alpha \rho_0 g \Delta T h^3}{\kappa \eta_0}. \quad (4)$$

We use  $Ra = 1.13 \times 10^7$  for all models which corresponds to a temperature contrast of 1300 K, a reference viscosity of  $1 \times 10^{20}$  Pa s, and the material parameters given in Table 1. Because the lithospheric plates are defined by a constant temperature, as opposed to half-space cooling, we use a reduced thermal expansivity ( $\alpha$ ) value of  $1.5 \times 10^{-5}$  K $^{-1}$  in order to give a reasonable bulk lithosphere-mantle density contrast of  $65 \text{ kg m}^{-3}$ . The domain size is  $7920 \text{ km} \times 1320 \text{ km} \times 13.2 \text{ km}$  (i.e. the computation is effectively 2-D). Both the subducting and OPs have initial uniform thicknesses of 80 km, and uniform initial temperature of 273 K ( $T_0$ ) (Fig. 1). In all models, subduction is initiated by prescribing an asymmetric lithospheric geometry in the trench region which provides the initial instability required for the lithosphere to freely subduct. This initial proto-slab extends to a depth of 150 km and has a radius of curvature of 200 km. The trench is initially located at  $x = 5000$  km and the plates extend to a distance of 500 km from the sidewalls. We also investigate slab dynamics in models where the OP trailing

edge is attached to the sidewall. Such models are termed ‘fixed OP’ models throughout the manuscript.

To facilitate decoupling of the SP from the OP, and the free-slip boundary, we insert a 15-km-thick, weak crustal layer within the SP which eradicates the need for plastic weakening at the trench (although the dynamic consequences of Byerlee yielding are examined in Section 3.4) (e.g. Běhouková & Čížková 2008; Stegman *et al.* 2010; Quinquis *et al.* 2011). The crust extends along the whole length of the SP and has a constant viscosity of  $0.2\eta_{\text{mant}}$  ( $= 2 \times 10^{19}$  Pa s). By holding the crustal properties constant throughout this study, we interpret variations in slab behaviour to be a result of the other parameters/rheologies explored (e.g. Androvicová *et al.* 2013). We have tested crustal viscosities below ( $\eta_c = \eta_{\text{mant}}/25$ ) and above ( $\eta_c = \eta_{\text{mant}}$ ) the chosen value, and find that reducing the viscosity increases both the SP and trench retreat velocities, but does not significantly modify the relative partitioning of subduction between these two components. Additionally, the morphological evolution of the slab is comparable for the crustal viscosities tested. We do not include a crust within the OP as we find that this typically gives rise to two-sided subduction (i.e. the OP detaches from the upper boundary). In the few models with an OP crust that do subduct in a one-sided fashion, we find that the slab dynamics, and large-scale OP stress state, are unchanged relative to the models with only a SP crust. Therefore, this approximation allows us focus on the processes associated with mature subduction, as opposed to the setup necessary to create the one-sided subduction observed on Earth.

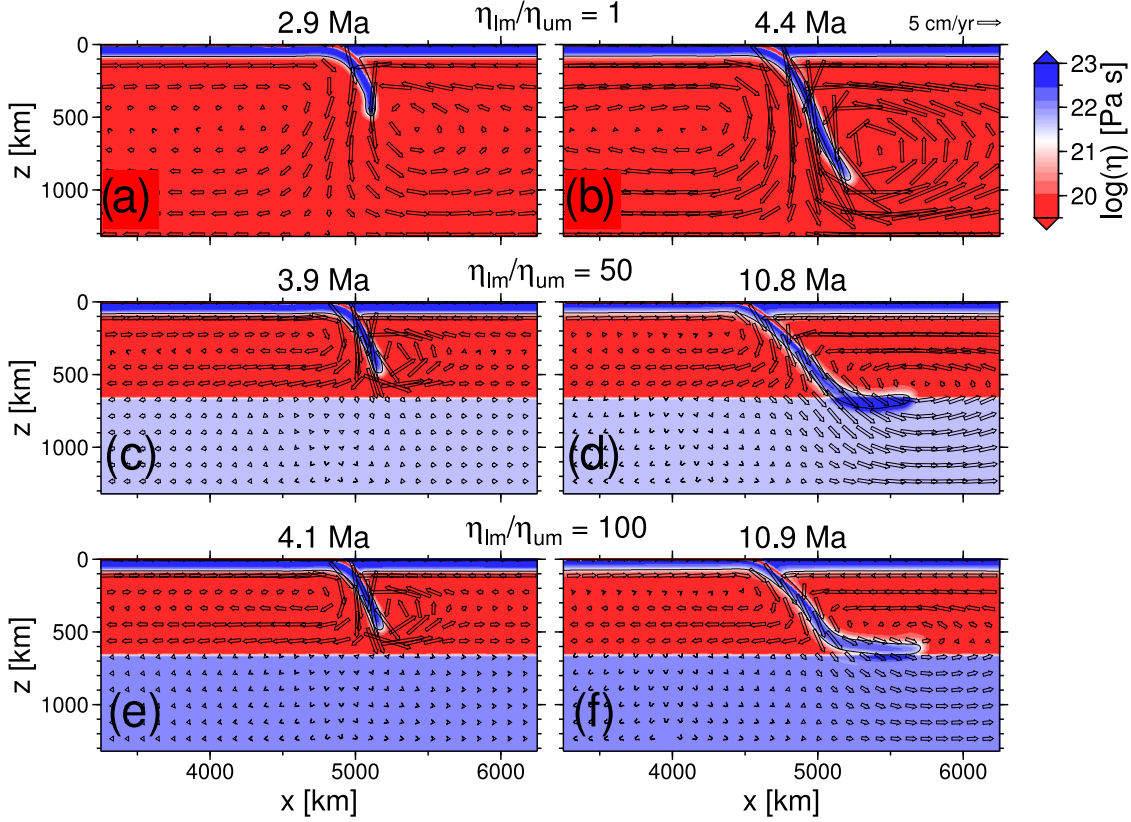


**Figure 2.** Viscosity field showing the evolution of the model without an upper-lower mantle viscosity contrast (a, b), and with viscosity contrasts of 50 (reference model: c, d), and 100 (e, f). All models have free OPs. The viscosity field shown here is a zoom in to the slab region. Overlain are velocity vectors.

The crust is defined using compositional tracers. Crustal properties are attributed to nodes that are above a certain compositional threshold,  $C_t$  (i.e. if  $C > C_t = 0.2$ ). Below 200 km depth, the crust is linearly tapered to zero thickness at mid-mantle depths. This tapering, as opposed to a sudden cutoff, is done to limit artificial stress discontinuities in the subducting lithosphere and is implemented by linearly increasing  $C_t$  from 0.2 at 200 km depth, to 1 at 660 km depth. The compositional material has no additional density component and is advected, using a marker tracing method, in the induced flow field:

$$\frac{\partial C}{\partial t} + \mathbf{u} \cdot \nabla C = 0. \quad (5)$$

40 compositional markers are initially contained within each of the cubic elements, and element dimensions vary from 5 km in the upper 330 km of the domain to 15 km elsewhere. We have tested that this element size is sufficient by ensuring that reducing the element size, by a factor of 2, does not modify the observed systematics, and has only a minor effect on the maximum sinking velocity (4 per cent increase).

The upper boundary has a constant temperature of 273 K ( $T_0$ ) and the base and sides have zero heat flux. Mechanically, all boundaries are free slip (reflecting). Such sidewall boundary conditions cause lateral confinement of the mantle flow which has been shown to promote reduced trench rollback, and slab folding atop a viscosity discontinuity, relative to models with periodic (Enns *et al.* 2005) or open side boundary conditions (Chertova *et al.* 2012). The use of a free slip upper boundary is an approximation to the true deformable free surface on Earth, which simplifies the numerics. This is likely to have only a minimal effect on slab dynamics as it has been shown that the use of a significantly weak crust allows the subducting

lithosphere to decouple from the surface, and bend, and so exhibit a similar behaviour to the equivalent model with a free surface (Quinquis *et al.* 2011).

## 2.2 Rheology

The first section of this work considers subduction in a setting where viscosity is solely a function of temperature. While experimental work (e.g. Karato & Wu 1993; Hirth & Kohlstedt 2003) suggests a complex dependence of viscosity on many parameters including pressure, water content, and grain size, we use a simple rheology in order to attempt to isolate and identify first-order effects on slab dynamics. We approximate the viscosity temperature-dependence as Frank-Kamenetskii (1969),

$$\eta_N = \eta_0 \exp[E(T_R - T)], \quad (6)$$

where  $T$  is the non-dimensional temperature, which varies between 0 and 1, and  $T_R$  is the non-dimensional reference temperature of 1. Our reference models use  $E = 6.2$ , which gives a maximum viscosity contrast, between the hottest and coldest material, of 500. Initially the lithosphere has a uniform temperature and so is isoviscous, as in compositional models. As the slab subducts, thermal diffusion causes the edges of the subducting slab to heat, and so weaken, while the core remains cool and retains its initial strength. The effective viscosity contrast during the free-sinking phase (e.g. Fig. 2c), taken as the viscosity contrast averaged over all nodes with  $T < 0.5$ , is reduced to  $\sim 350$  which is compatible with the range of effective viscosity contrasts of 100–500 estimated from observables such as minimum radii of curvature, and plate-trench kinematics (Becker

et al. 1999; Conrad & Hager 1999; Funiciello *et al.* 2008; Wu *et al.* 2008; Stegman *et al.* 2010).

The use of a Frank-Kamenetskii rheology with such a low  $E$  is a significant approximation to laboratory-derived Arrhenius rheologies which would suggest that lithospheric viscosities are  $\sim 20$  orders of magnitude greater than the underlying mantle (equivalent  $E \sim 45$ ) (e.g. Frank-Kamenetskii 1969; Karato & Wu 1993; Hirth & Kohlstedt 2003). Such high lithospheric strengths are, however, likely limited by plastic failure. In our models, including a rheology with an equivalently strong temperature-dependence, and a maximum viscosity cut-off, gives rise to issues regarding the obtainment of stable subduction. The subducting slab cools the region of the mantle wedge adjacent to the subducting crust which, for a strongly temperature-dependent viscosity, results in strong material above weak crust connecting the two plates. This results in sluggish plate motions, and an OP stress state that is affected by the gravitational pull of the additional material located above the crust. At the expense of limiting rheological realism, we avoid these non-physical effects by reducing the temperature-dependence of the viscosity. Our simplified rheology allows us to easily probe the first order effects of various lithospheric properties, without slab stability issues.

We also examine the dynamic effects of a stress-dependent viscosity, in which there is a power-law relationship between stress and strain rate in the upper mantle ( $z < 660$  km). For simplicity, we assume that the power-law viscosity has an exponential temperature dependence with an exponential factor equivalent to that of the Newtonian viscosity ( $E$ ) divided by the power-law exponent ( $n$ ). This allows the power-law viscosity ( $\eta_P$ ) to be written in terms of the Newtonian viscosity ( $\eta_N$ ):

$$\eta_P = k_P \dot{\epsilon}_{II}^{\frac{1-n}{n}} \eta_N^{\frac{1}{n}}. \quad (7)$$

Here,  $\dot{\epsilon}_{II}$  is the second invariant of the strain rate tensor, and  $k_P$  is a constant pre-factor. We use  $n = 3.5$  to approximate the stress-dependence of viscosity in the dislocation creep regime. Prescribing a transition stress,  $\sigma_T$ , at which the power law and Newtonian strain rates are equal allows the constant in eq. (7),  $k_P$ , to be expressed as a function of  $\sigma_T$  and  $n$ . Assuming the total strain rate is the sum of the Newtonian and power-law components, a joint Newtonian/power-law viscosity is then computed as follows:

$$\frac{1}{\eta_{eff}} = \frac{1}{\eta_N} + \frac{1}{\eta_P}. \quad (8)$$

Inserting the two viscosity components into eq. (8) then gives an effective viscosity ( $\eta_{eff}$ ) which is dominantly Newtonian (eq. 6) at stresses below  $\sigma_T$ , and power law (eq. 7) at stresses above  $\sigma_T$ :

$$\eta_{eff} = \frac{\eta_N}{1 + \left(\frac{2\dot{\epsilon}\eta_N}{\sigma_T}\right)^{1-\frac{1}{n}}}. \quad (9)$$

We also test how the inclusion of a viscoplastic rheology, which approximates brittle deformation in the lithosphere (e.g. Schott & Schmeling 1998), modifies slab dynamics relative to the purely viscous reference. In this case, the effective viscosity is composed of a Newtonian (eq. 6) and a plastic term (eq. 11):

$$\frac{1}{\eta_{eff}} = \frac{1}{\eta_N} + \frac{1}{\eta_{yield}}, \quad (10)$$

where the plastic viscosity is calculated as follows:

$$\eta_{yield} = \frac{\tau_{yield}}{2\dot{\epsilon}_{II}}. \quad (11)$$

The yield stress,  $\tau_{yield}$ , is defined by Byerlee's friction relationship (Byerlee 1968):

$$\tau_{yield} = (a\sigma_l + b)\lambda, \quad (12)$$

where  $\sigma_l$  is the lithostatic pressure ( $= \rho_0 g z$ ),  $b$  and  $a$  are constants (see Table 1), and  $\lambda$  is a pore pressure pre-factor which is not well constrained. We restrict plastic yielding to lithospheric depths ( $z < 80$  km), and use  $\lambda = 0.15$ . This value of the pre-factor results in significant plastic weakening, yet does not weaken the trench region completely, and is comparable to that favoured in previous studies [e.g. Enns *et al.* (2005): 0.1, Di Giuseppe *et al.* (2008): 0.08].

### 3 RESULTS

First, we present our reference model with a Newtonian rheology and characterize the effect of the OP, and upper-lower mantle viscosity contrast on the evolution of the subducting slab. We then explore the role of the lithospheric–sublithospheric mantle viscosity contrast, and stress-dependent rheologies, on our reference model with a mobile OP. Finally, for the Newtonian reference model, we focus on the role of the OP mechanical properties for models with both free and fixed OPs.

#### 3.1 Reference model and role of viscosity stratification

The morphological evolution of the subducting slab is affected by the vertical viscosity structure. Fig. 2 shows the reference model with a uniform viscosity mantle (top panel) compared with two other models in which the viscosity increases by a factor of 50 (middle panel) and 100 (lower panel) at the transition between the upper and lower mantle ( $z = 660$  km). The temporal evolution of the slab sinking ( $V_Z$ ), trench retreat ( $V_T$ ) and SP velocities ( $V_P$ ) are shown in Fig. 3, for the models with mid-mantle viscosity increases of factors 50 (green line) and 100 (blue). The uniform viscosity mantle model is omitted from the kinematics plot, as it requires a vastly stretched velocity axis (i.e. maximum  $V_Z = 33$  cm yr $^{-1}$ ). Also shown in Fig. 3 are the kinematics for models with fixed (black) and absent OPs (red), which are discussed in the subsequent section.  $V_T$  is computed by tracking the rightmost location of the crustal material at the surface, and  $V_P$  is computed by tracking the position of the trailing edge of the SP.

Irrespective of the vertical viscosity structure of the mantle (Fig. 2), the slab initially sinks freely and the lithosphere unbends to increase the radius of curvature initially imposed. The sinking velocity increases due to the increasing slab pull force, until the slab begins to feel the viscosity increase/lower boundary (Fig. 3a). At this time, the slab begins to slow and curve upwards due to the viscous drag exerted by the lower mantle/boundary, which causes a reduction in the upper-mantle slab dip angle. In the interest of conciseness, we subsequently refer to the average upper mantle slab dip angle as simply the slab ‘dip’. The imposed lithosphere–mantle viscosity contrast is too low to favour a subduction mode in which the trench advances, and so the trench retreats throughout subduction (e.g. Ribe 2010; Stegman *et al.* 2010). Subduction is partitioned approximately equally between trench retreat and plate advance, with both components increasing as the magnitude of the slab pull force increases during the free-sinking phase (Fig. 3b). Because the slab is retreating rapidly during its descent through the upper mantle ( $V_T \sim 5$  cm yr $^{-1}$ ), it has a substantially inclined slab dip (Figs 2c and e). In addition to the slab’s reasonably low viscosity, and the absence of phase transition-related density effects, this low dip angle causes

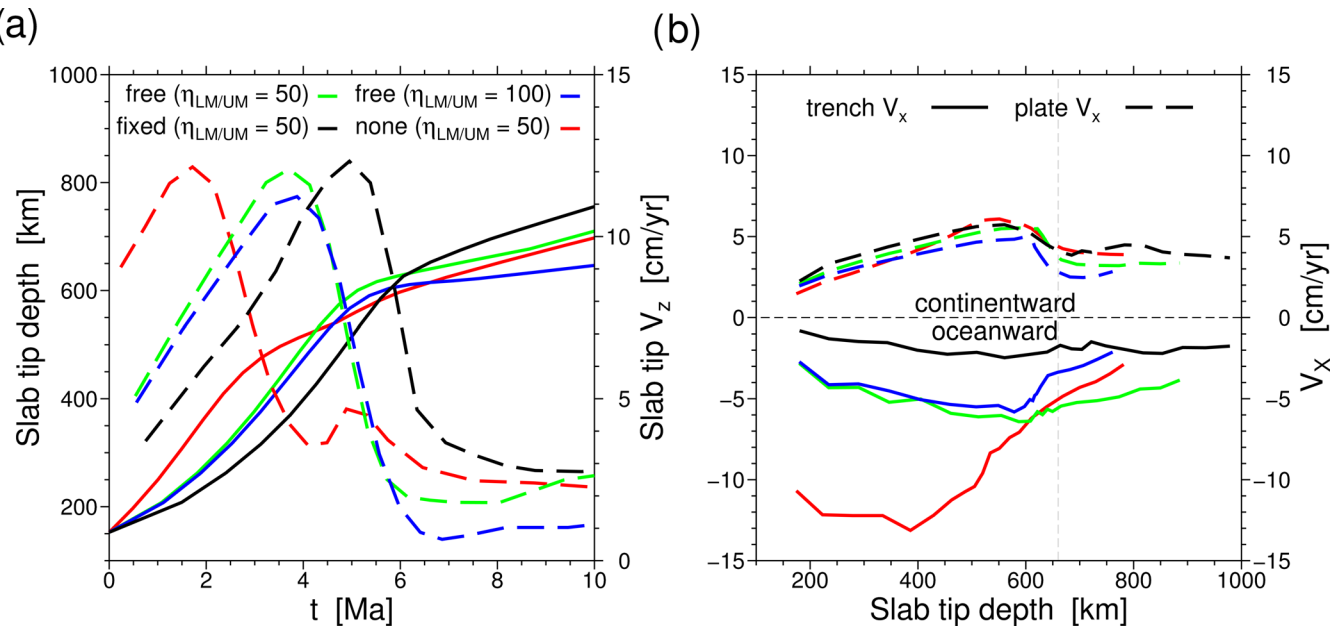


**Figure 3.** Kinematic evolution of models with variable mid-mantle viscosity contrasts (green  $\eta_{LM}/\eta_{UM} = 50$ , blue:  $\eta_{LM}/\eta_{UM} = 100$ ), model without an overriding plate (red), and model with a fixed overriding plate (black). Shown is, (a), slab tip depth (solid line) and vertical velocity (dashed) versus time and, (b), subducting plate (dashed line) and trench velocity (solid) as a function of slab tip depth.

the slab to flatten horizontally above the viscosity discontinuity, and then slowly sink into the lower mantle (Fig. 2d; e.g. Christensen 1996; Čížková *et al.* 2002; Enns *et al.* 2005). Upon interaction of the slab tip with the viscosity increase/lower boundary, both the plate advance and trench retreat velocities decrease.

The evolution of the OP, and SP bending region, stress field for models with a uniform viscosity mantle, and with a factor 50 viscosity increase, are shown in the top four rows of Fig. 4. As we mainly focus on the stress state of the flat-lying OP, we plot the horizontal deviatoric stress. While the amplitudes and spatial positions of the highly stressed regions vary, the style of OP stress is comparable for the free OP models with and without a mid-mantle viscosity increase (Figs 4a–g). The highest stresses, of  $>50$  MPa, are found within the lithosphere, particularly within the trench bending region where there is extension above, and compression below, the horizontal mid-plane of the subducting lithosphere. Comparably large stresses also occur below the trench where downdip extension occurs due to the slab pull force. In the OP, stresses are maximum in the forearc region where horizontal compression occurs, and at distances of greater than  $\sim 300$  km from the plate interface where extension occurs (e.g. Tagawa *et al.* 2007a; Capitanio *et al.* 2010a; Nakakuki *et al.* 2010; Schellart & Moresi 2013).

At the time-step prior to interaction with the viscosity discontinuity, both models have fore-arc compression (layered model:  $\sim 10$  MPa, non-layered:  $\sim 20$  MPa) in the OP at close proximity to the trench (Figs 4a and e). While fore-arc compression is located at equivalent positions, extensional stresses are focused at different distances away from the trench in the models with and without a stratified mantle. Extensional stresses of  $\sim 20$  MPa are centred at  $\sim 750$  km from the trench for the layered viscosity case, and  $\sim 1000$  km from the trench in the model without a stratified mantle. As well as being centred at a larger distance from the trench, the region of significant extensional stress is also broader in the model without a viscosity jump. As the slab descends in the model without a viscosity jump, the amplitude of both compression and extension increases (both to  $\sim 40$  MPa) as the vigour of

mantle flow increases due to increased subduction velocities, yet they do not vary in terms of relative magnitude. In contrast to this, the OP stresses in the layered viscosity model have a strong time dependence. As the slab interacts with the viscosity increase and rollback velocity decreases, a shift from dominantly OP extension to dominantly OP compression occurs (Figs 4e and g). This spatial variability in the degree of OP extension between models, and how it evolves temporally, correlates with the style of mantle flow below the OP, suggesting a basal traction origin for the observed extension (Section 4.1.3).

### 3.2 Effect of overriding plate

The presence of an OP limits the vertical extent of the poloidal flow cell and increases the depth at which the fastest, trench-directed horizontal mantle flow occurs. The top row of Fig. 5 shows the slab morphology in the model without an OP. Relative to the model with a free OP, the slab dip angle is reduced in the single plate case (cf. Figs 2c and 5a). This reduced dip occurs in part because the trench retreat velocity is greater during the free-sinking stages for the single plate model, relative to the model with an OP (Fig. 3b; e.g. Yamato *et al.* 2009; Butterworth *et al.* 2012). In the model without an OP, subduction occurs dominantly via trench retreat (i.e.  $V_T \gg V_P$ ). Inclusion of a free OP results in subduction that is partitioned approximately equally between plate advance and trench retreat (Fig. 3b).

The inclusion of an OP limits the vertical extent of large scale mantle wedge flow, and places strong and dense material adjacent to the SP hinge. In order to determine which of these OP effects causes slabs that are subducting beneath OPs to behave so differently from those in isolation, we examine models in which the OP is separated from the SP by a weak crust and an additional region of mantle material (e.g. Yamato *et al.* 2009), relative to the reference model where the plates are separated by only the weak crust (e.g. Capitanio *et al.* 2010a). We refer to the model with mantle material between

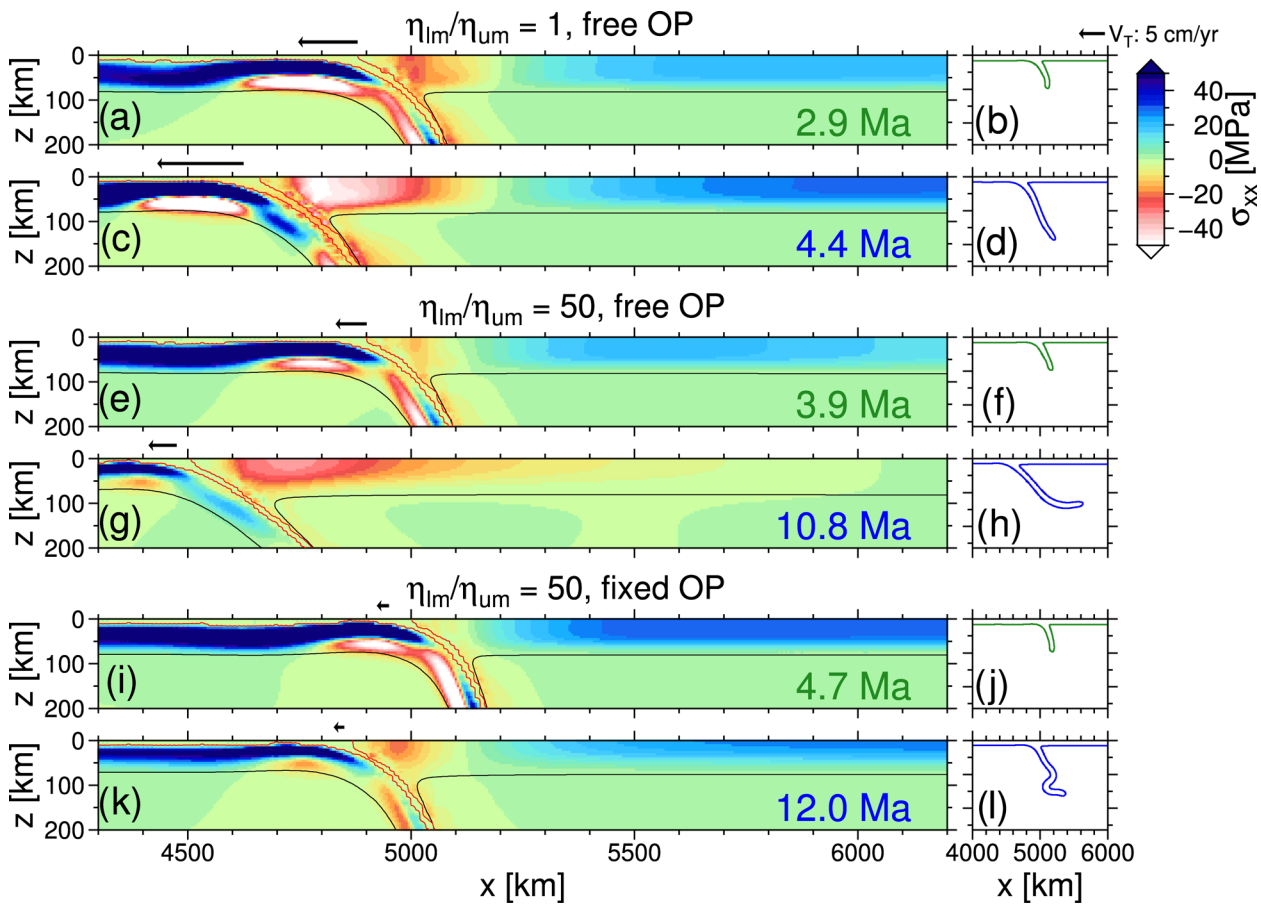


**Figure 4.** Horizontal deviatoric normal stress in the trench region and OP for model with a free OP and no upper-lower mantle viscosity contrast (a–d), reference model with a free OP and upper-lower mantle viscosity contrast of 50 (e–h), and model with a fixed OP and upper-lower mantle viscosity contrast of 50 (i–l). Negative values (red) correspond to compression, and positive values to tension (blue). Panels to the right show slab isotherms to illustrate the slab morphology, and a vector scaled by the trench retreat velocity is plotted above the trench.

the SP and OP as the ‘shallow mantle wedge’ model (Figs 5c and d). The upper mantle slab dip in the shallow mantle wedge model is comparable to that in the reference model with an OP (*cf.* Figs 2c and 5c). In align with this, the average trench retreat velocity in the shallow wedge model (not shown) is comparable to that of the reference model with an OP, albeit slightly elevated ( $\sim 5 \text{ cm yr}^{-1}$  relative to  $\sim 4 \text{ cm yr}^{-1}$ ). Thus, while trench retreat is driven by the slab’s negative buoyancy, the presence of an OP reduces the tendency of the slab to retreat at its high, single plate rate whether or not the OP is directly adjacent to the SP.

However, whether the SP is in direct contact with the OP or not does exert a strong control on the OP stress regime. Significant OP forearc compression ( $\geq 20 \text{ MPa}$ ) only occurs when the OP is directly adjacent to the SP, as return flow-induced basal tractions drag the OP into the SP. In the decoupled models, compression is concentrated in the thermal boundary layer which develops above the region of shallow mantle. The basal traction-driven OP extension is, however, comparable in both extent and amplitude ( $\sim 20 \text{ MPa}$ ).

Models in which the OP trailing edge is attached to the side of the domain, termed ‘fixed’ OP models here, exhibit trench retreat velocities that are further reduced ( $V_T = 2 \text{ cm yr}^{-1}$ ). This is because rollback requires thinning of the OP. This gives rise to slabs with large dip angles which fold and penetrate into the lower mantle (Fig. 5f). The OP stress state in the fixed OP model is dominated by high extensional stresses ( $\sim 35 \text{ MPa}$ ), relative to the free OP case ( $\sim 20 \text{ MPa}$ ), due to the rollback-driven OP stretching (*cf.* Figs 4e

and i). As observed in previous work, the OP stress state oscillates between periods of intense and more minor extension as the slab folds, and the rollback rate oscillates (Clark *et al.* 2008; Capitanio *et al.* 2010a,b). While the partitioning of subduction between  $V_T$  and  $V_P$  is strongly modified by the presence and mobility of the OP, it is found that the maximum sinking velocity ( $V_Z \sim 12 \text{ cm yr}^{-1}$ ) does not depend on how the OP is modelled (*i.e.* absent, free, or fixed).

### 3.3 Plate viscosity

We now investigate the role of lithospheric viscosity in our two-plate Newtonian models by analysing models with plates that have lower ( $\eta' = \eta_{\text{slab}}/\eta_{\text{mantle}} = 100$ ) and higher viscosities ( $\eta' = 2000$ ) than in the reference models ( $\eta' = 500$ ). The relatively low viscosity plate models are often referred to as ‘weak’ and the relatively high viscosity models as ‘strong’ throughout the text. Fig. 6 illustrates the slab morphologies of the lithospheric viscosity end-member models for both free (left-hand panel) and fixed OPs (right-hand panel), and the associated SP kinematics are shown in Fig. 7. Here, for both the free (black) and fixed OP (red) models, characteristic velocities are plotted as a function of lithospheric strength. The maximum trench retreat, plate, and slab tip sinking velocities are extracted, for periods before ( $z_{\text{slab}} < 630 \text{ km}$ ) and after ( $z_{\text{slab}} > 690 \text{ km}$ ) the slab has reached the upper-lower mantle viscosity discontinuity, from time

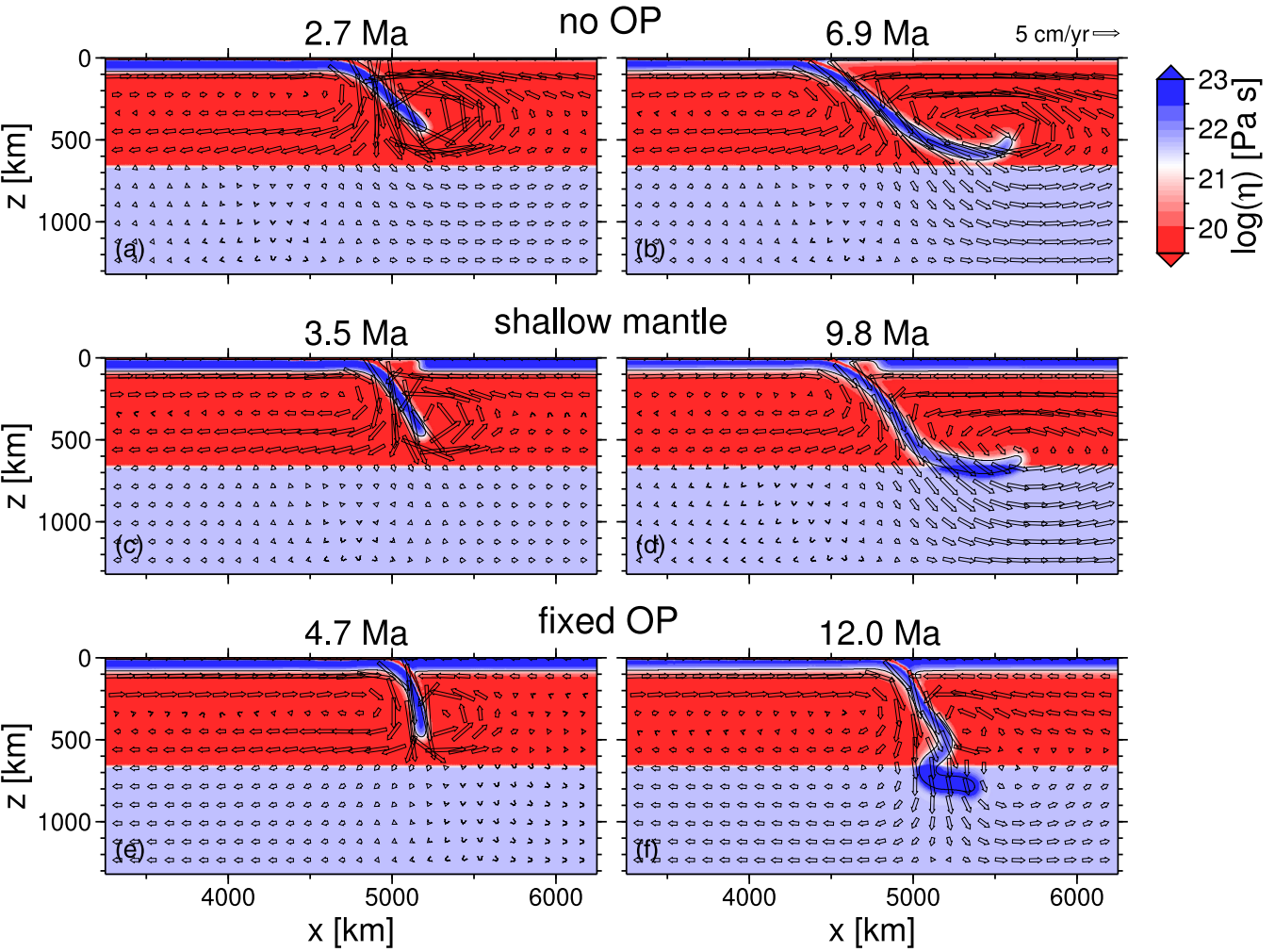


**Figure 5.** Viscosity field showing the evolution of a model without an overriding plate (a, b), with a free overriding plate separated from the subducting plate by an initially 300 km wide region of mantle material (c, d), and with an overriding plate fixed to the side of the domain (e, f).

series such as those shown in Fig. 3. Additionally, the maximum trench–plate velocity ratio, which relates to how the subduction velocity is partitioned between slab rollback and plate advance, is plotted as a function of plate strength. We have verified that using the mean velocity, as an alternate metric, does not change the systematics observed.

We find that the slab in the intermediate viscosity reference model ( $\eta' = 500$ ; Fig. 2d) has a lower dip angle than both the strong and weak slabs (Figs 6a and c), a trend also observed in the equivalent models without an OP (not shown). In the strong plate model, the slab can penetrate into the high viscosity lower mantle, which results in a relatively high dip angle throughout subduction. The slab in the weak plate model has an increased dip angle during the later phase of subduction due to the strong reduction in rollback that the slab experiences as it impinges on the mid-mantle viscosity jump (e.g. Zhong & Gurnis 1995; Enns *et al.* 2005). Fig. 7(a) shows that, during the free sinking phase (filled circles), rollback velocity increases with decreasing plate viscosity. As mentioned above, there is a significant reduction in the retreat velocity in the lower mantle for the weak slabs. However, the trench retreat velocity of the stronger slabs, which penetrate more easily through the viscosity contrast, is only slightly reduced (Fig. 7a).

Slab rollback in the models with fixed OPs occurs at the expense of OP thinning and so trench retreat is slower than in the free

models for all plate viscosities (Fig. 7a). There is a greater disparity in rollback rates, and slab dips, between the free and fixed OP cases for the strong plate models ( $\Delta V_T/V_{T,\text{free}} \approx 0.70$ ), relative to the weak models ( $\Delta V_T/V_{T,\text{free}} \approx 0.45$ ) (Fig. 7a). The SP velocity ( $V_P$ ) shows less variability (Fig. 7b). The anomalously high  $V_P$  data points, during the latter phase ( $z_{\text{slab}} > 690$  km) for the weak plate model ( $\eta' = 100$ ), occur because subduction begins to initiate at the SP trailing edge. For both the free and fixed OP cases, the strong plate models are observed to have significantly reduced slab sinking velocities (Fig. 7d). The maximum sinking velocity, of  $\approx 16$  cm yr $^{-1}$  for  $\eta' = 100$  and  $\approx 8$  cm yr $^{-1}$  for  $\eta' = 2000$ , is unaffected by whether the OP is free to move (e.g. Capitanio *et al.* 2010a; Meyer & Schellart 2013).

The lithospheric viscosity exerts a strong control on the stress regime of the OP (Fig. 8). In addition to the general trend of increased forearc compression as the slab reaches the mid-mantle viscosity jump for all models, there is a switch from OPs dominated by forearc compression ( $\sim 30$  MPa) in the weak plate model, to OPs that are dominantly extensional ( $\sim 40$  MPa) in the strong plate model (Fig. 8). The amplitude of the convergence velocity between the trench and the trailing edge of the OP ( $V_{\text{op}} - V_T$ ), which corresponds to either net OP extension (negative convergence velocity) or net OP compression (positive), is plotted for the free OP models in Fig. 9(a). For the weaker plate models, the rate of trench

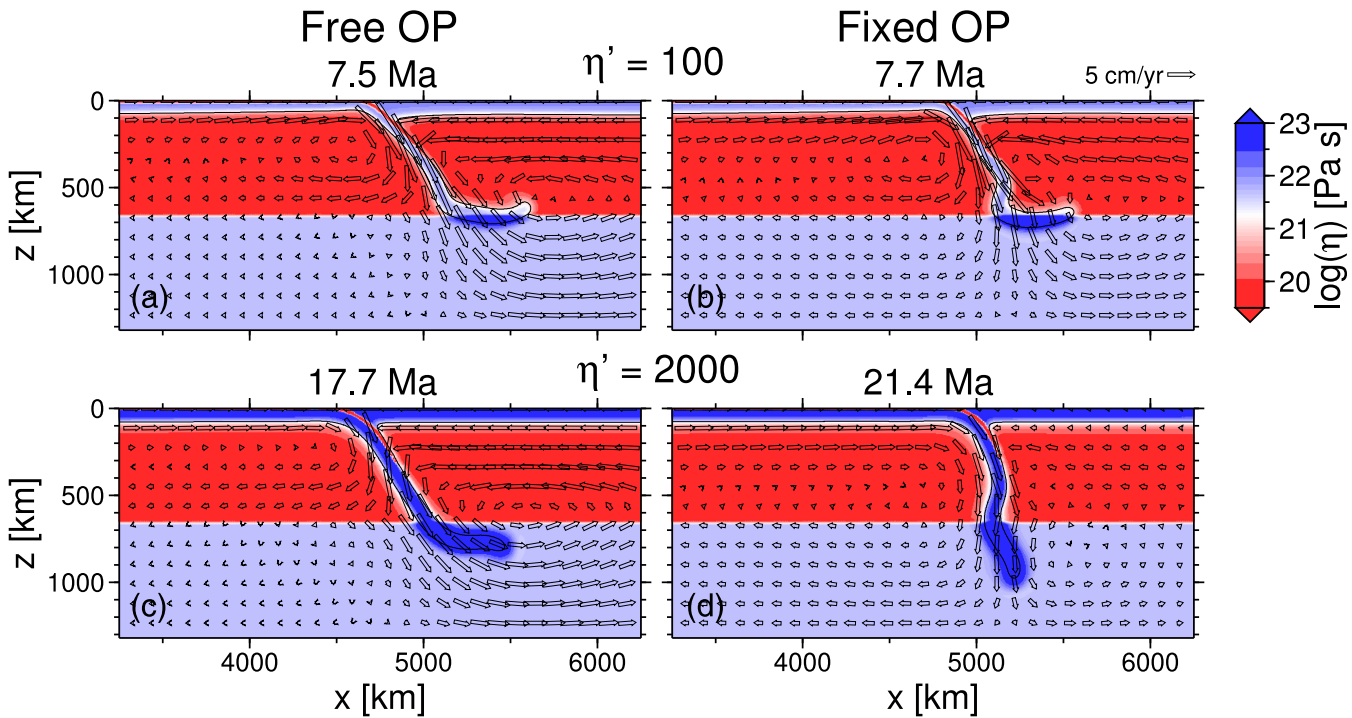


**Figure 6.** Viscosity field, during the latter stages of subduction, for models with variable plate-mantle viscosity contrasts ( $\eta'$ ). Left-hand panels show cases in which the OP is free (a, c), and right-hand panels show fixed OP models (b, d).

retreat decreases significantly as the slab feels the viscosity increase mid-mantle depths, while the trenchward OP velocity decreases at a much slower rate. This results in net convergence, as is seen in the stress field (Fig. 8c), during the later stages of subduction. In contrast to this, the trench retreat velocity in the strong plate model continues to increase as the slab sinks into the lower mantle. This results in an OP trailing edge with net motion away from the trench (i.e. negative  $V_{op} - V_T$ ) for the duration of subduction, which gives rise to net OP extension (Fig. 9a). Despite having a much lower amplitude convergence velocity ( $0.2\text{--}0.6 \text{ cm yr}^{-1}$ ) than the weak plate model (up to  $4.5 \text{ cm yr}^{-1}$ ), the strong plate model has comparable OP stresses because the convergence velocity scales with horizontal strain rate.

In order to determine the degree of control that the OP viscosity has on the subducting slab dynamics and OP stress regime, relative to the role of the SP viscosity, we have additionally tested the effect of varying solely the OP viscosity ( $\eta'_{op} = 100, 2000$ ). For the free OP models, reducing the OP viscosity does not have a strong effect on the subducting slab morphology. Slabs in the low viscosity OP model do rollback slightly faster ( $\Delta V_T \approx 1 \text{ cm yr}^{-1}$ ), which results in a minor reduction in the dip angle (not shown). As for the models in which the viscosity of both plates is varied, the variability in slab morphology between the free and fixed OP models is much greater for the high viscosity OP models. In contrast to the switch from compression to extension observed when the viscosity of the SP is also varied, the viscosity of the OP does not significantly modify the OP stress state during either the free-sinking or flattening phases. This suggests that it is the viscosity of the SP which exerts the strongest control on the OP stress state for the free OP models.

### 3.4 Stress-dependent rheologies

Having examined the effects of varying the viscosity of the entire lithosphere, we now investigate how the inclusion of stress-

dependent rheologies, which focus viscosity weakening in regions of high deformation, modify subducting slab kinematics and OP stress in our free OP model. We explore the effect of a power-law rheology (eqs 7–9) with a power-law exponent ( $n$ ) of 3.5, and a Newtonian rheology with Byerlee plasticity (eqs 10–12). We use a transition stress ( $\sigma_T$ ) of 100 MPa, which puts the low stress, ambient mantle within the diffusion creep regime, and the deforming lithosphere in the dislocation creep regime. While a value of 100 MPa is comparable to that used in previous studies which parameterize the Newtonian-power law transition by a constant stress [e.g. McNamara *et al.* (2001): 70 MPa], there is considerable uncertainty regarding the appropriate value of this tuning parameter, and its dependence on temperature, pressure and composition. We therefore examine its effect at the end of this section. In these models, the mantle immediately surrounding the slab is dominantly in the Newtonian regime. This is not the case for studies that use more complex, laboratory derived rheologies (e.g. Billen & Hirth 2005, 2007; Nakakuki & Mura 2013; Garel *et al.* 2014), and the dynamic implications of this are discussed in Section 4.2.1.

The morphological effect of including a power law rheology is shown in Figs 10(a) and (b). The greatest stresses occur within the strong lithosphere, and so here the model is in the power law regime. Maximum weakening, relative to the Newtonian viscosity, of a factor of  $\sim 10$  occurs at the trench where the bending stresses are maximum. Additionally, triggered by extensional stresses, the surface portion of the SP is in the power law regime with relative viscosity reductions extending from the bending region and monotonically decreasing towards the trailing edge. As the slab reaches the mid-mantle (Fig. 10b), the slab pull force is, in part, supported by the high viscosity lower mantle, and so the degree of relative weakening is reduced in the subducting slab/plate. In accordance with the evolution of the OP stress state (Figs 12a and c), minor weakening occurs in the extensional backarc during the free-sinking phase, and more significant weakening occurs in the compressional

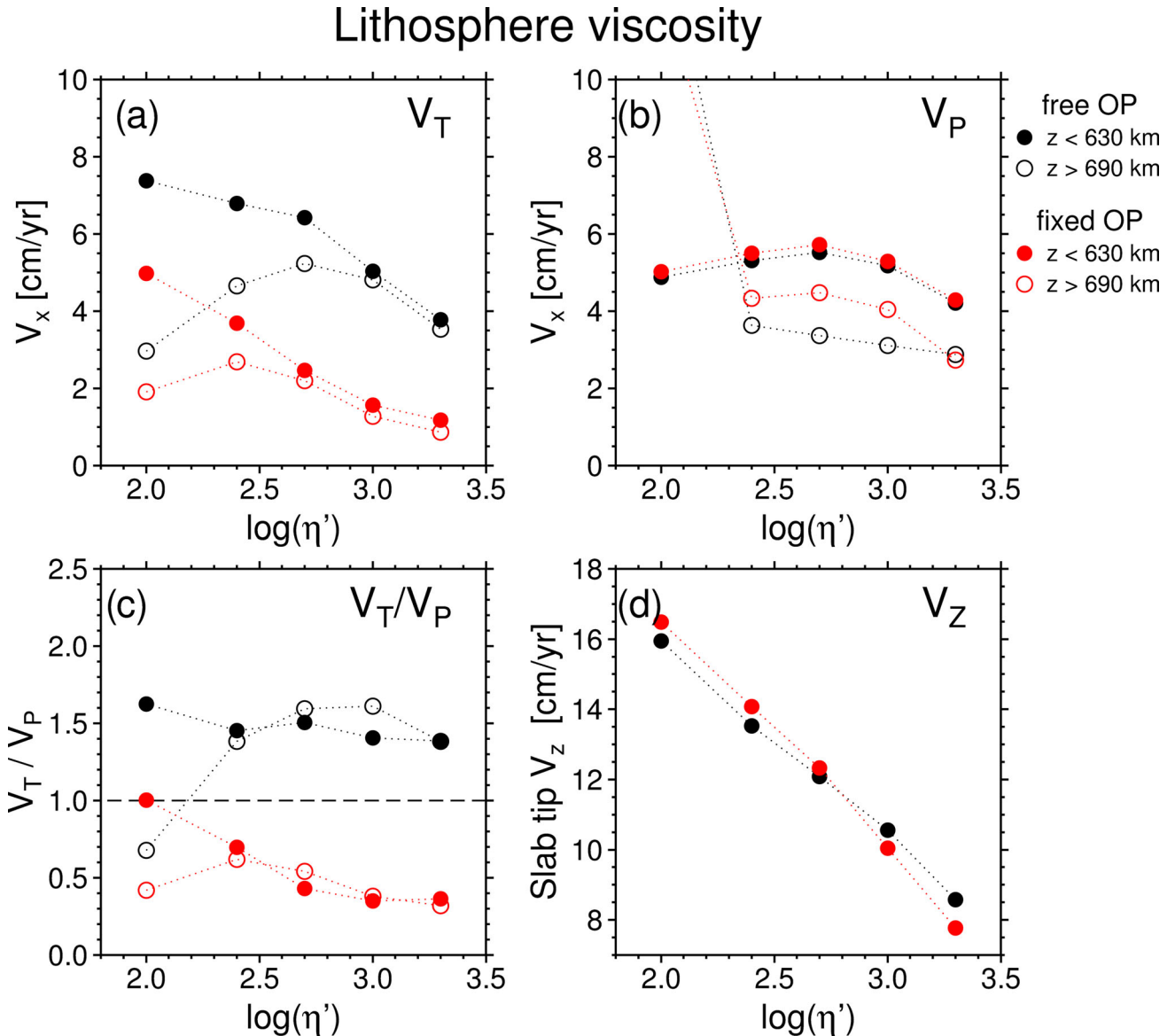


**Figure 7.** Dependence of subducting plate kinematics on plate-mantle viscosity contrast ( $\eta'$ ). Diagnostic velocities are taken as the maximum upper mantle (slab tip  $z_{\text{slab}} < 630$  km: filled circles) and lower mantle velocities ( $z_{\text{slab}} > 690$  km: hollow circles), for both the free (black circles) and fixed overriding plates (red circles) (see Fig. 6). Shown is: (a) the maximum upper and lower mantle trench velocity, (b) plate velocity (c), trench-plate velocity ratio and (d), vertical slab tip velocity. The reference model corresponds to  $\log(\eta') = 2.69$ .

forearc once the slab has reached the mid-mantle. In the viscoplastic model (Figs 10e–f), viscosity weakening is of greater magnitude, more spatially localized and, due to the linear increase in  $\tau_{\text{yield}}$  with depth, only at shallow lithospheric depths (e.g. Čížková *et al.* 2007). As seen in single plate models, the strongest plastic weakening is triggered by extensional bending stresses, and occurs in the surface portion of the SP at a distance of  $\sim 150$  km from the trench (e.g. Enns *et al.* 2005; Di Giuseppe *et al.* 2008).

The peak sinking velocity ( $V_z$ ) of the models with viscosity weakening is substantially higher ( $15\text{--}16 \text{ cm yr}^{-1}$ ) than for the equivalent Newtonian reference model ( $\approx 12 \text{ cm yr}^{-1}$ ; Fig. 11a). Because viscosity reductions in the surrounding mantle are minor, such elevated  $V_z$ , as in the model with a weak SP (Fig. 7d: for  $\eta'_{\text{op}} = 100$ ,  $V_z \approx 16.5 \text{ cm yr}^{-1}$ ), is due to a reduction in the bending region viscosity, which reduces the subduction-resisting plate bending force. Within the upper mantle, the SP velocity ( $V_p$ ) and, to a greater degree, the trench retreat velocity ( $V_T$ ) are elevated with respect to

the reference model ( $\Delta V_T \approx 1.5 \text{ cm yr}^{-1}$ ,  $\Delta V_p \approx 0.75 \text{ cm yr}^{-1}$ ). This results in slab dips that are slightly reduced relative to the Newtonian reference (cf. Figs 10a and 2c). After interaction with the high viscosity lower mantle, as in the weak slab model (Fig. 7a), the initially elevated rollback rate is reduced to below that of the Newtonian reference, particularly for the model with a power law rheology (Fig. 11b). This gives rise to an increase in slab dip in the power-law model, relative to the Newtonian reference (cf. Figs 10b and 2d).

The inclusion of stress-dependent weakening modifies the OP stress regime relative to the Newtonian reference. In both the power law and viscoplastic models, the OP is under greater forearc compression (15–25 MPa), and there is a reduced region of significant backarc extension (250 km), relative to the Newtonian model (compression of  $\sim 10$  MPa, and extension over  $\sim 700$  km) (cf. Figs 4 and 12). This trend persists when slabs reach the mid-mantle viscosity discontinuity, with significant  $\geq 10$  MPa compression

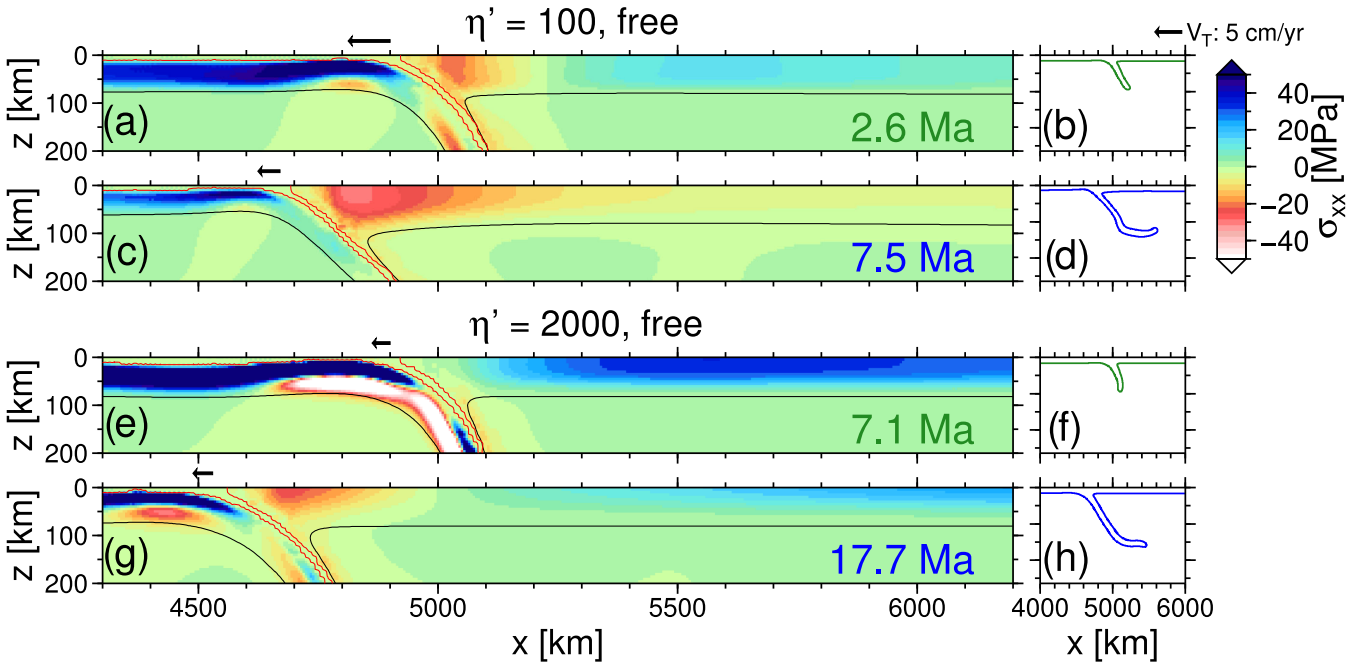


**Figure 8.** Evolution of the horizontal deviatoric normal stress in the trench region and OP for models with variable plate-mantle viscosity contrasts and a free OP (see Fig. 6). Upper panels (a–d) show the weak plate model ( $\eta' = 100$ ) and lower panels (e–h) show the strong plate model ( $\eta' = 2000$ ). For detailed caption (see Fig. 4).

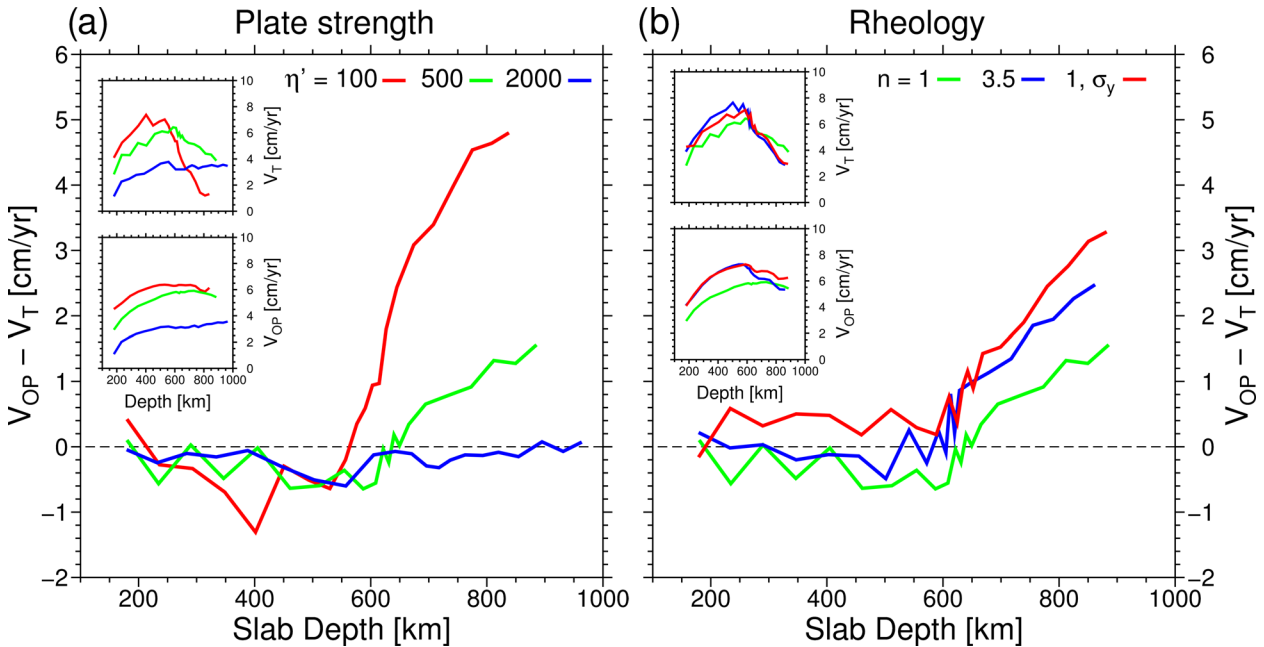


**Figure 9.** Convergence velocity between the trench ( $V_T$ ) and the trailing edge of the overriding plate ( $V_{OP}$ ) plotted as a function of slab tip depth for free OP models with, (a), variable plate-mantle viscosity contrasts (see Fig. 6) and, (b), rheologies (see Fig. 10). Small inset panels show the evolution of the two individual components,  $V_T$  and  $V_{OP}$ . Negative convergence velocity corresponds to net OP extension, and positive convergence velocity corresponds to net OP compression.

extending over a wider region (>1600 km) than in the reference model (~900 km). This tendency towards a compressive OP for models with stress-dependent rheologies is concurrent with elevated trench-OP convergence throughout the duration of subduction (Fig. 9b). The model with Byerlee plasticity exhibits the greatest amplitude forearc compression (~40 MPa), which follows from the elevated convergence velocity (Fig. 9b). Additional features in the OP stress field include reduced bending stresses in the SP relative

to the Newtonian models, and the focusing of highly stressed regions at greater depths for the model with plasticity (Fig. 12g; e.g. Čížková *et al.* 2007).

We now consider the transition stress,  $\sigma_T$ , which is used to tune the regions of the model which undergo power law deformation. We have examined the effect of reducing  $\sigma_T$  to 50 MPa (Figs 10c and d) and increasing  $\sigma_T$  to 150 MPa for models with  $n = 3.5$  and a free OP. Reducing  $\sigma_T$  accentuates power law deformation

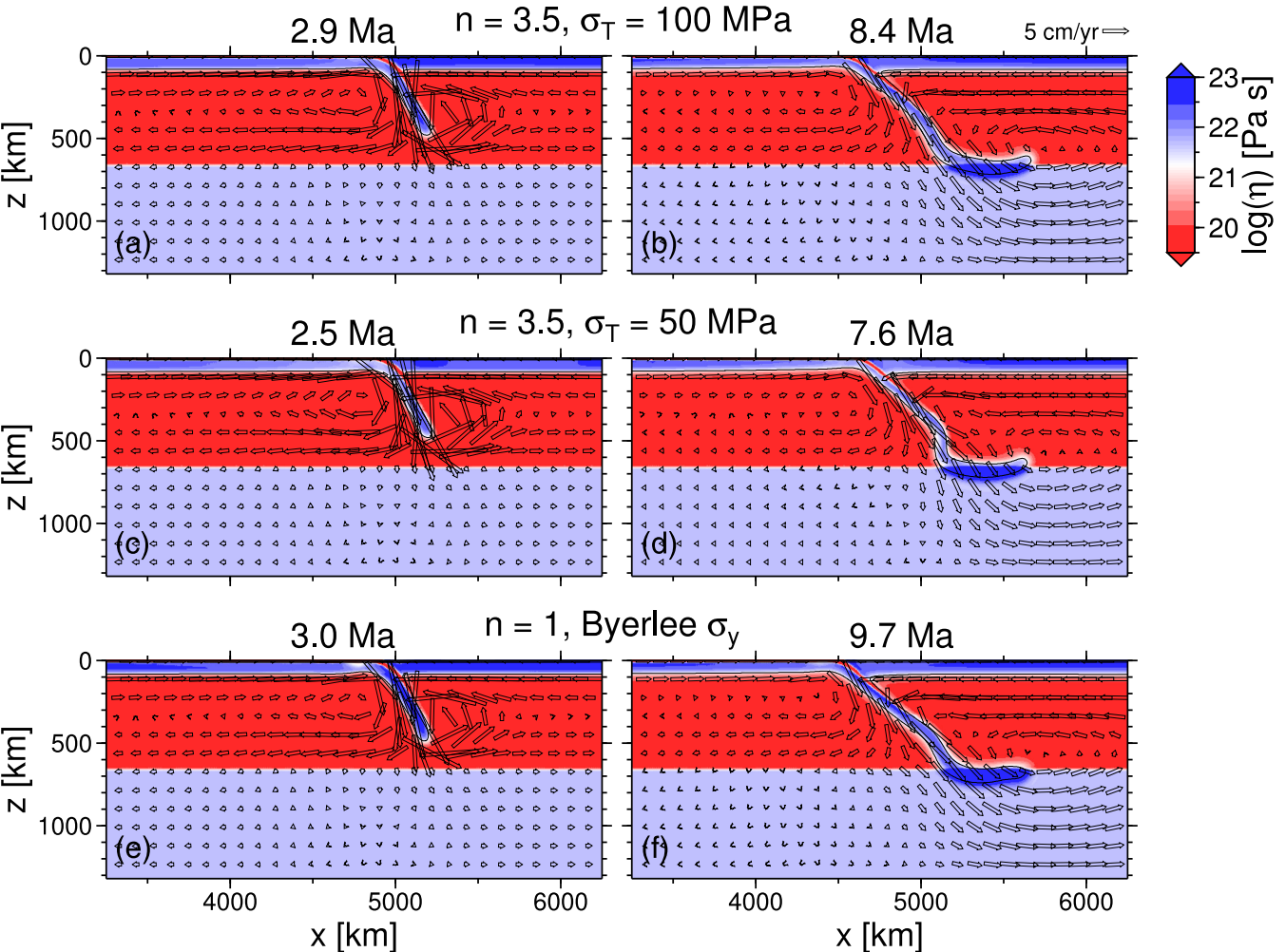


**Figure 10.** Slab evolution for free OP models with power law (a–d) and viscoplastic (e, f) rheologies. The top two rows show power law models with an exponent ( $n$ ) of 3.5, and transition stresses of 100 MPa (a, c) and 50 MPa (c, d). The bottom row shows the visco-plastic model with a depth-increasing Byerlee yield stress (e, f).

in the bending region, where the degree of viscosity weakening is greater in magnitude, but less localized in space. During the free sinking phase, reducing the transition stress to 50 MPa enables OP weakening, relative to the Newtonian case, in the back-arc and fore-arc simultaneously. Reducing  $\sigma_T$  also promotes a reduction in slab rollback, and slab buckling, upon slab interaction with the lower mantle. Conversely, increasing  $\sigma_T$  to 150 MPa results in an OP that undergoes only very minor weakening throughout the duration of subduction, and has a slab morphology similar to the Newtonian reference.

### 3.5 Overriding plate thickness

We now return to the Newtonian rheology models to investigate the role of the OP thickness and density, on the dynamics of the subducting slab and the OP stress regime. In order to target the role of the OP, the mechanical properties of the SP are kept constant throughout this section ( $\eta'_{sp} = 500$ ,  $h_{sp} = 80$  km,  $\rho_{sp} - \rho_m = 65$  kg m $^{-3}$ ).

Firstly, we examine the effect of the OP thickness ( $h_{op}$ ) on the subducting slab. Figs 13(a)–(d) shows slabs with relatively thin (40 km) and thick OPs (120 km), during the slab flattening phase. For the free OP case, subduction below a thinner OP results in a

decrease in slab dip (Fig. 13a). In analogy to the single plate case, this reduction in slab dip stems from an increase in slab rollback that occurs because a thin OP suppresses the ‘free’ rate of trench retreat less than a thick OP. For the fixed OP models, we also find that increasing  $h_{op}$  reduces  $V_T$  and increases slab dip. As is the case for increasing the OP viscosity, this effect is stronger when the OP is fixed, as  $V_T$  is controlled by the OPs resistance to uniaxial stretching. Therefore, models with high viscosity or thick OPs have similar slab morphologies, with near-vertical dip angles and penetration into the lower mantle (Fig. 13d).

This strong dependence of trench retreat on OP thickness is shown in Fig. 14(a), for both free and fixed OPs. The maximum trench retreat rate decreases with increasing OP thickness (free OP in upper mantle, for  $h_{op} = 40$  km;  $V_T \approx 8.0$  cm yr $^{-1}$ , for  $h_{op} = 120$  km;  $V_T \approx 5.2$  cm yr $^{-1}$ ), except during the latter stages of the free OP models, where  $V_T$  is strongly affected by slab interaction with the viscosity discontinuity. The SP velocity ( $V_P$ ) is insensitive to OP thickness and so  $V_T/V_P$  generally decreases with increasing  $h_{op}$ , owing to the reduction in  $V_T$ . It is found that, despite significant variation in the partitioning of subduction between  $V_T$  and  $V_P$ , the maximum slab sinking velocity of  $\sim 12$  cm yr $^{-1}$  is not affected by  $h_{op}$  (e.g. Capitanio *et al.* 2010a; Duarte *et al.* 2013; Meyer & Schellart 2013). In agreement with previous work, the amplitude of

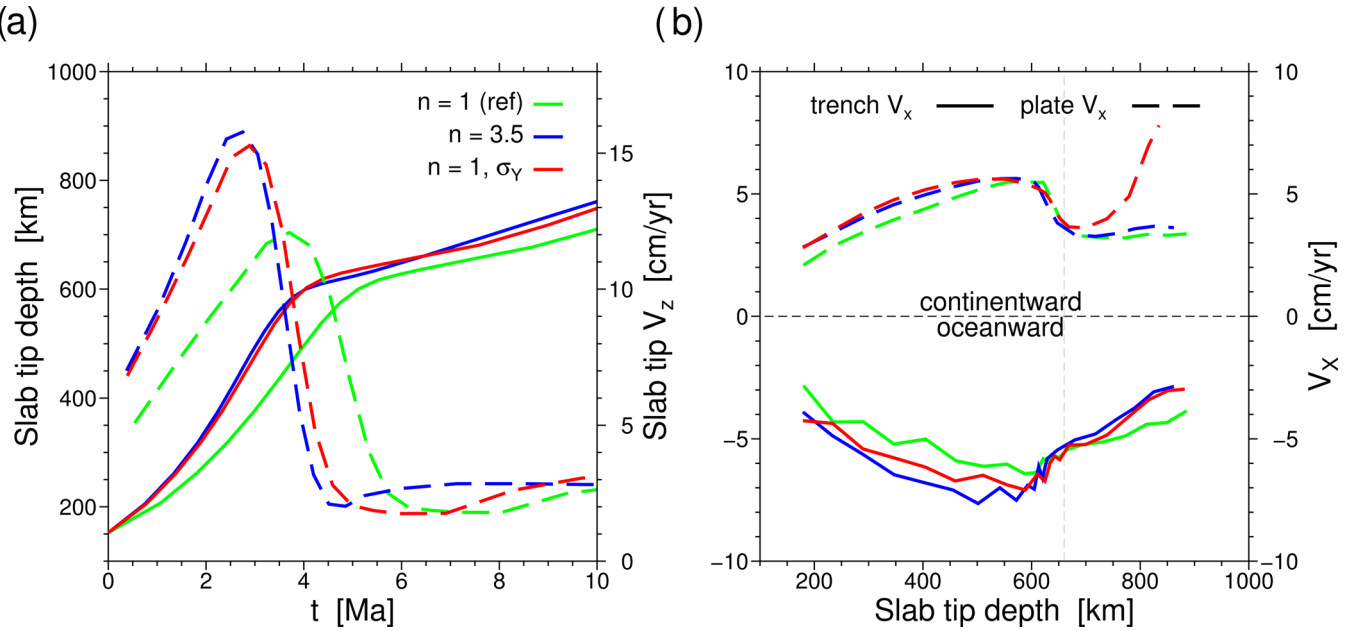


**Figure 11.** Kinematic evolution of free OP models with stress-dependent rheologies (see Fig. 10). Shown is: (a) slab tip depth (solid line) and vertical velocity (dashed) versus time and (b) subducting plate (dashed line) and trench velocity (solid) as a function of slab tip depth.

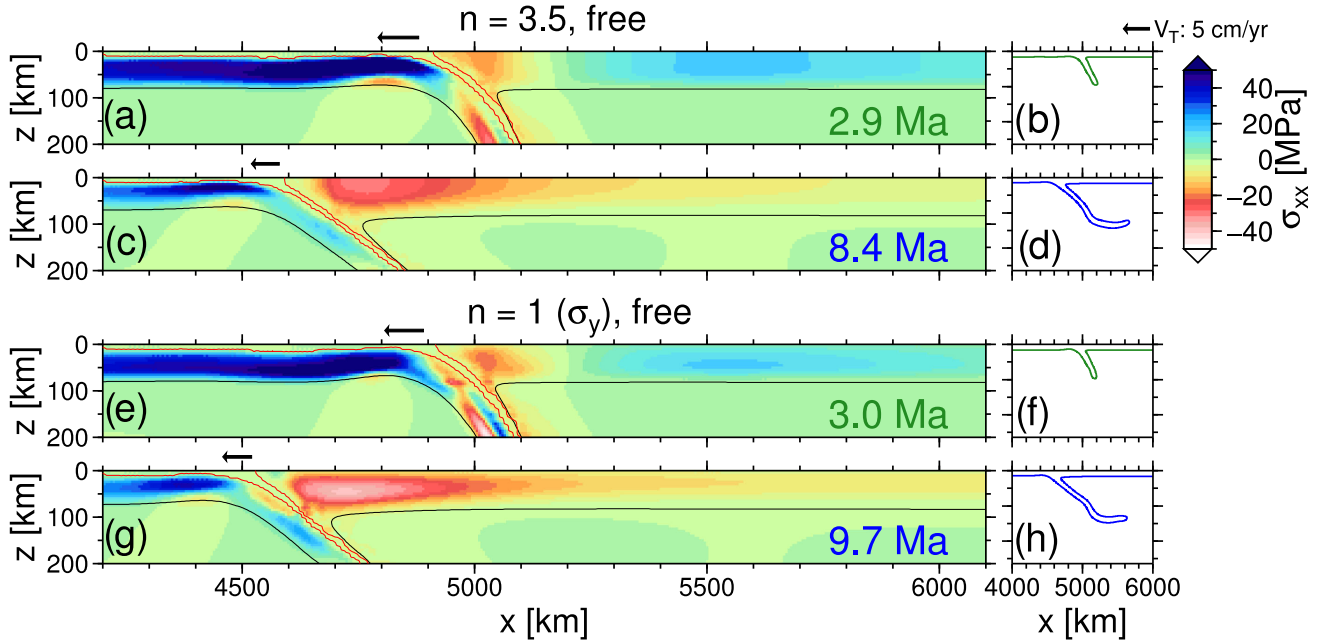


**Figure 12.** Evolution of the horizontal deviatoric normal stress in the trench region and overriding plate for models with stress-dependent rheologies and a free OP (see Fig. 10). Upper panels (a–d) show the  $n = 3.5$ , power law model ( $\sigma_T = 100$  MPa), and the lower panels (e–h) show the viscoplastic model with a depth-increasing Byerlee yield stress. For detailed caption see Fig. 4.

OP stresses depends strongly on the thickness of the OP. The thick OP models have reduced maximum extensional and compressional stress amplitudes because trench rollback is preferentially accommodated by OP motion/translation, rather than thinning/thickening as in the thin OP model (Capitanio *et al.* 2010a, 2011; Meyer & Schellart 2013).

### 3.6 Overriding plate density

We now examine the role of OP buoyancy, the density contrast between the OP and surrounding mantle ( $\Delta\rho_{\text{op}} = \rho_{\text{op}} - \rho_m$ ), for a fixed

SP buoyancy ( $\Delta\rho_{\text{sp}} = \rho_{\text{sp}} - \rho_m = 65$  kg m $^{-3}$ ). Figs 13(e)–(h) shows slabs with positively buoyant ( $\Delta\rho_{\text{op}} = -130$  kg m $^{-3}$ ), neutrally buoyant ( $\Delta\rho_{\text{op}} = 0$ ), and negatively buoyant ( $\Delta\rho_{\text{op}} = 130$  kg m $^{-3}$ ) OPs. It is apparent that decreasing the buoyancy of the OP significantly reduces the dip angle of the subducting slab, particularly for the case in which the OP is fixed at its lateral edge. Upon examining the kinematics, it can be seen that for all models, and during both phases of subduction (i.e. lower and upper mantle), maximum trench retreat velocity increases as slab buoyancy decreases (e.g. free OP model in upper mantle: For  $\Delta\rho_{\text{op}} = 130$  kg m $^{-3}$ ;  $V_T \approx 6.4$  cm yr $^{-1}$ , and for  $\Delta\rho_{\text{op}} = -130$  kg m $^{-3}$ ;  $V_T \approx 8.7$  cm yr $^{-1}$ ; Figs 14c and

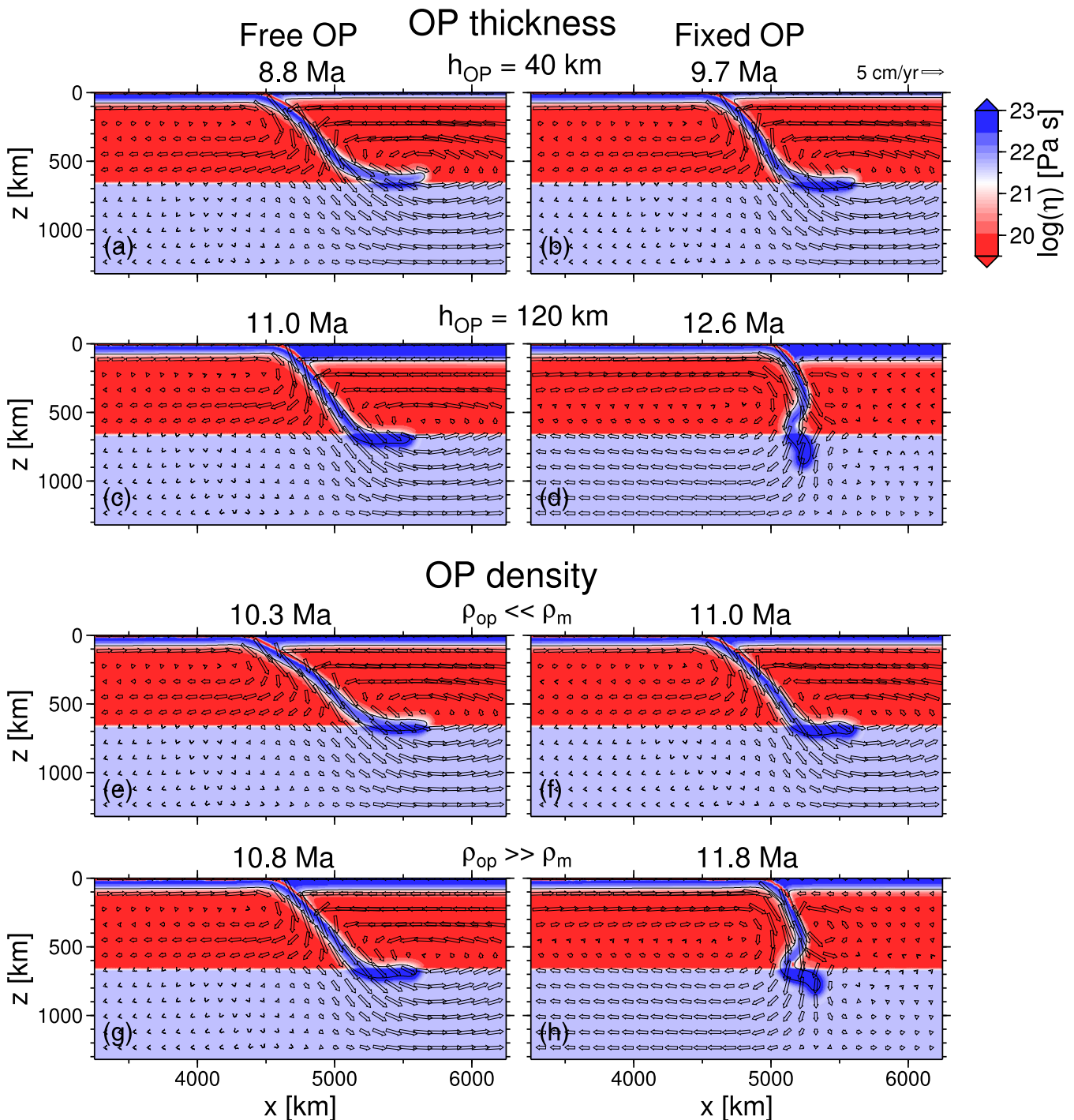


**Figure 13.** Viscosity field, during the latter stages of subduction, for models with variable overriding plate thickness ( $h_{\text{op}}$ ) and overriding plate buoyancy ( $\rho_{\text{op}} - \rho_m$ ). Shown are models with thin OPs ( $h_{\text{op}} = 40 \text{ km}$ : a and b) thick OPs ( $h_{\text{op}} = 120 \text{ km}$ : c and d), positively buoyant OPs ( $\rho_{\text{op}} - \rho_m = -130 \text{ kg m}^{-3}$ : e and f) and negatively buoyant OPs ( $\rho_{\text{op}} - \rho_m = 130 \text{ kg m}^{-3}$ : g and h). Left-hand panels show cases in which the OP is free (a, c, e, g), and right-hand panels show fixed OP models (b, d, f, h).

d). The SP velocity remains relatively constant as it is controlled by the buoyancy and strength of the subducting slab, which is held constant here (i.e.  $V_p \approx 5.5 \text{ cm yr}^{-1}$  for all  $\Delta\rho_{\text{op}}$ ). The increase in rollback velocity for positively buoyant OPs occurs because the lateral density increase, across the trench from OP to SP, results in a pressure gradient directed in the SP direction. Such elevated slab rollback reduces the dip angle of the slab (*cf.* Figs 13e and g).

Conversely, the reduced  $V_T$  for slabs with negatively buoyant OPs results in an increased slab dip angle. This effect is more prominent for the fixed OP models, where the slab dip transitions from  $\sim 45^\circ$  in the positively buoyant OP model to near vertical in the negatively buoyant OP model (Figs 13f and h).

The OP buoyancy has a very strong effect on the OP stress regime, as is shown in Fig. 15 for the free OP models. There is a

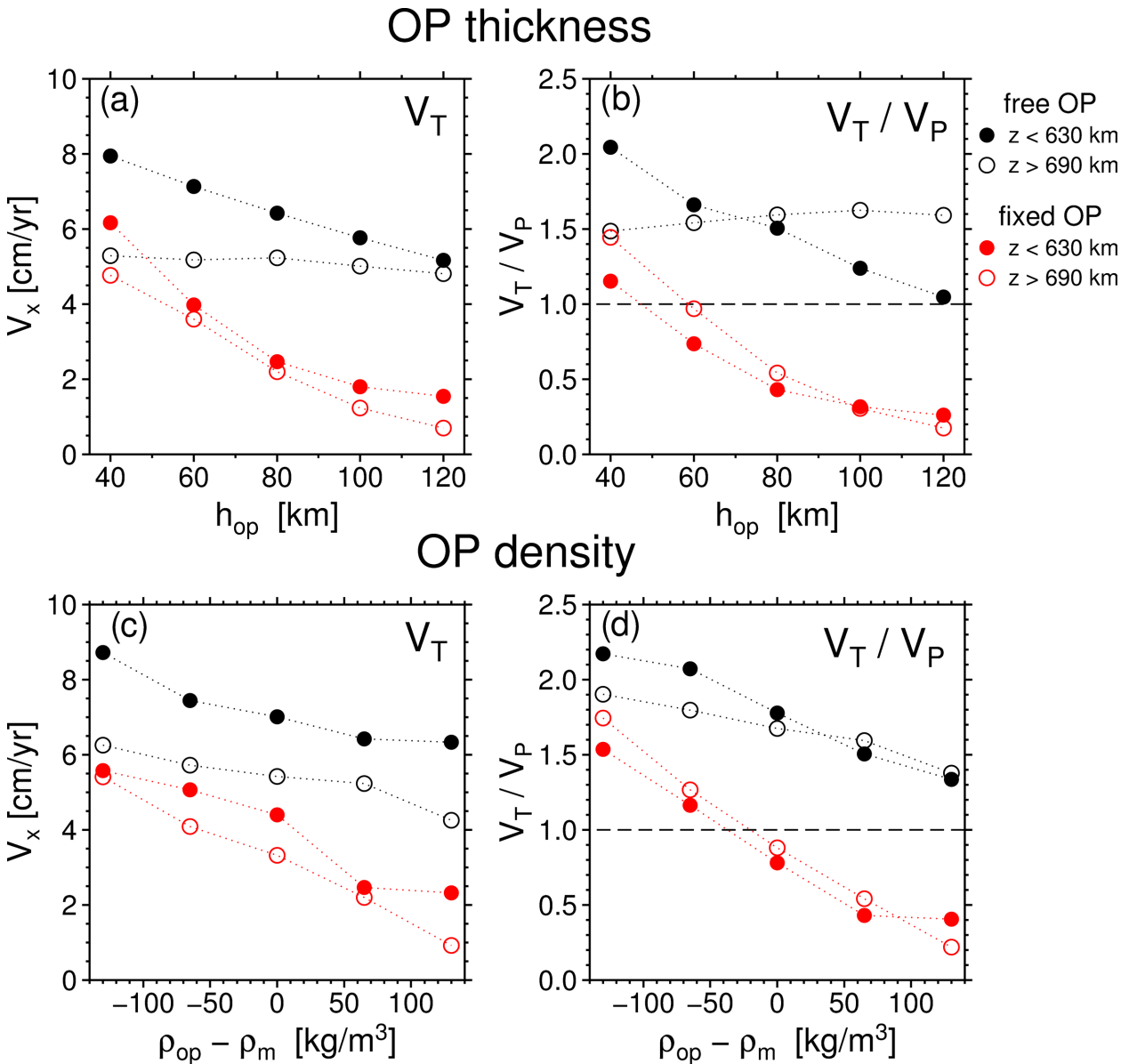


**Figure 14.** Dependence of trench retreat on overriding plate thickness ( $h_{op}$ ) and overriding plate density ( $\Delta\rho_{op} = \rho_{op} - \rho_m$ ) (see Fig. 13). Shown is the maximum upper (filled circles) and lower mantle (hollow circles) trench velocity (a, c), and trench-plate velocity ratio (b, d). Note, reference model corresponds to  $h_{op} = 80$  km =  $h_{op}$ , and  $\Delta\rho_{op} = 65$  kg m<sup>-3</sup>.

transition from purely OP extension in the positively buoyant OP model, to concurrent forearc compression and backarc extension in the neutrally buoyant OP model, and then purely compression in the negatively buoyant OP model. The reference model, with  $\Delta\rho_{op} = 65$  kg m<sup>-3</sup>, has an OP density, and so OP stress regime and slab rollback velocity (Figs 4e–h) midway between the negatively buoyant and neutrally buoyant OP models shown (Fig. 15).

## 4 DISCUSSION

### 4.1 General features

#### 4.1.1 Role of overriding plate

We observe slab rollback in all of our models and find that the presence of a free OP reduces the maximum trench retreat velocity

by a factor of  $\sim 2$ . This observation is in agreement with previous modelling work by Yamato *et al.* (2009) and Butterworth *et al.* (2012). Previous dynamic subduction models with an OP either consider two plates that are separated by only a thin, weak crust (e.g. Capitanio *et al.* 2010a; Schellart & Moresi 2013; Garel *et al.* 2014) or a larger region containing mantle material (e.g. Yamato *et al.* 2009; Butterworth *et al.* 2012). Whether the OP and SP are separated only by crust, or crust and a region of mantle material (i.e. ‘shallow mantle wedge’ models), does not significantly modify the trench retreat rate or slab dip angle. This suggests that the reduced slab dip angle in the single plate models is a result of the restriction of large-scale vertical flow, and not the presence of lithospheric plate adjacent to the SP/crust. The presence of mantle material adjacent to the SP hinge in the shallow mantle wedge model does, however, result in trench retreat that is slightly elevated relative to the reference OP model ( $\Delta V_T \approx 1$  cm yr<sup>-1</sup>). This is due to the SP-directed pressure gradient arising from the lateral density

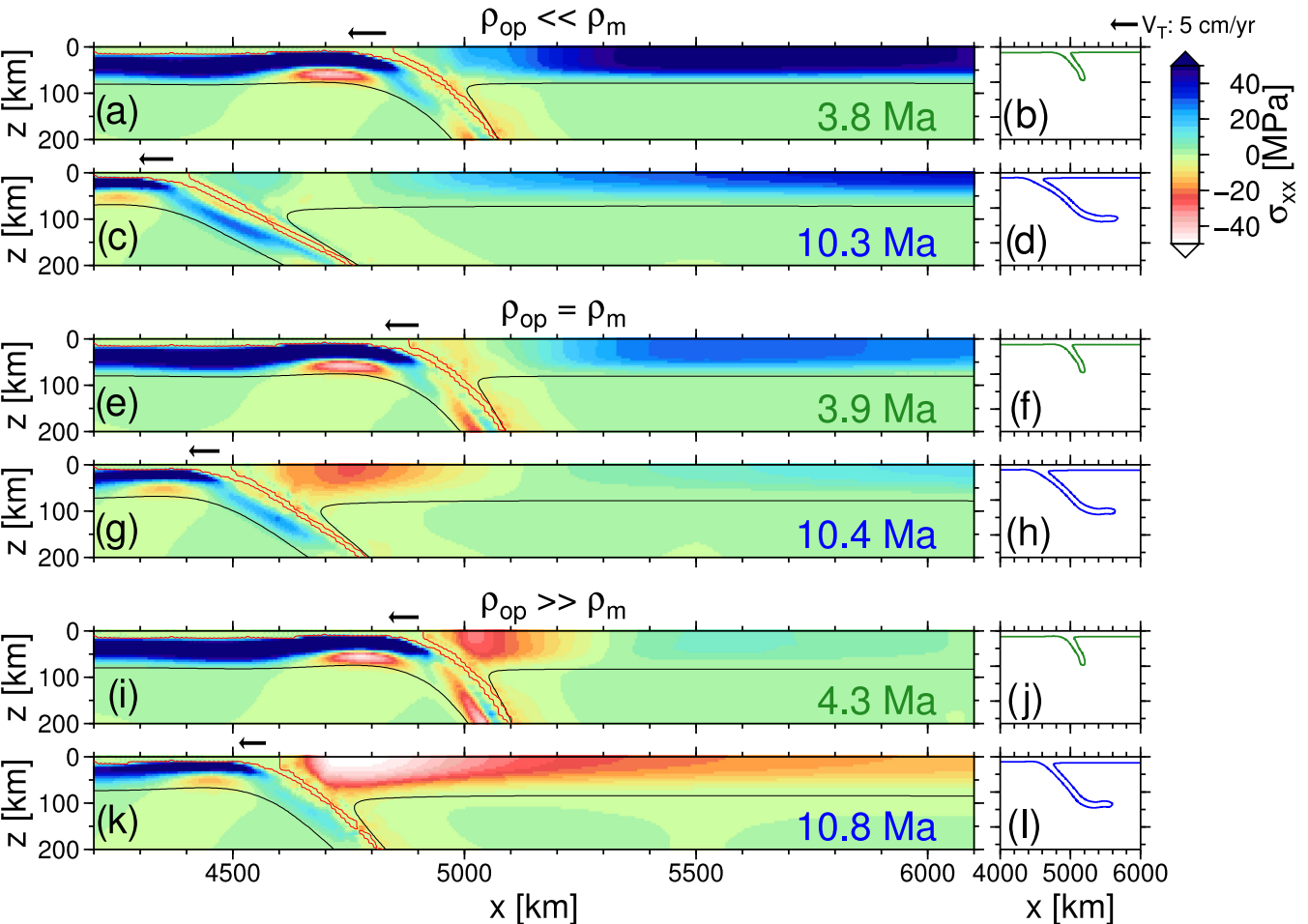


**Figure 15.** Evolution of the horizontal deviatoric normal stress in the trench region and overriding plate for models with variable overriding plate buoyancy and a free OP (see Fig. 13). Upper panels (a–d) show the positively buoyant overriding plate model ( $\rho_{\text{op}} - \rho_m = -130 \text{ kg m}^{-3}$ ), centre panels (e–h) show the neutrally buoyant OP model ( $\rho_{\text{op}} = \rho_m$ ), and lower panels (i–l) show the negatively buoyant OP model ( $\rho_{\text{op}} - \rho_m = 130 \text{ kg m}^{-3}$ ). For detailed caption, see Fig. 4.

increase from wedge to SP. This effect is of importance in models with variable  $\rho_{\text{op}}$ , and is discussed in more detail in Section 4.2.2, but is of secondary importance relative to the vertical restriction of large-scale mantle flow.

We find that the OP does not significantly affect plate advance velocity ( $V_P$ ), and so the presence of an OP alters the partitioning of subduction between plate advance and trench retreat by reducing  $V_T$  to a value comparable to  $V_P$  (i.e. reduces  $V_T / V_P$ ). This is consistent with previous modelling work (Capitanio *et al.* 2010a; Schellart & Moresi 2013), and the observation that, in nature, trench motion is typically smaller than plate motions (e.g. Heuret & Lallemand 2005). Thus, while rollback is ‘slab-driven’ in our models of free subduction (e.g. Elsasser 1971; Kincaid & Olson 1987; Stegman *et al.* 2006; Schellart 2008a), it is affected by the OP and its mechanical properties even in models where the OP is free to move. In contrast, Capitanio *et al.* (2010a) find that the presence of a free OP does not modify how subduction is partitioned between rollback and plate advance. As other parameter values are comparable, this is potentially due to the very strong SP core ( $3000\eta_{\text{mantle}}$ ) used by Capitanio *et al.* (2010a), which increases the stiffness of the SP hinge. As is observed in previous two-plate modelling studies (e.g. Capitanio *et al.* 2010a; Meyer & Schellart 2013), the vertical sinking velocity ( $V_z$ ) is unaffected by the style of OP. This suggests that the mechanical properties of the SP, namely the negative buoyancy and

hinge stiffness ( $\propto$  plate viscosity  $\times$  thickness<sup>3</sup>, for an isoviscous plate), control slab sinking (Conrad & Hager 1999).

When the slab subducts beneath an OP that is fixed to the edge of the box, which is perhaps analogous to a large continental OP with low plate velocity (Forsyth & Uyeda 1975), we find that rate of trench retreat is significantly reduced (e.g. Capitanio *et al.* 2010a,b). This occurs because, in models with fixed OPs, slab rollback is inhibited by the tensile strength of the OP (Ribe 2001:  $\propto \eta'_{\text{op}} h_{\text{op}}$ ), as the OP must be stretched for rollback to occur. Therefore, a fixed OP exerts a much stronger control on slab rollback than a free OP, further reducing  $V_T$  from its single plate rate (e.g. Capitanio *et al.* 2010a,b).

#### 4.1.2 Role of viscosity stratification

In our reference model, we include a factor 50 increase in the background viscosity at a depth of 660 km by increasing the prefactor in our viscosity law (eq. 6; e.g. Enns *et al.* 2005; Garel *et al.* 2014). For simplicity, we do not include other phase transitions, and the associated density/buoyancy effects (e.g. Tagawa *et al.* 2007a,b; Nakakuki *et al.* 2010; Nakakuki & Mura 2013), which have been shown to promote slab folding atop 660 km (Cížková & Bina 2013). Even without density effects, which tend to inhibit penetration through

the mid-mantle discontinuity, we find the a  $\times 50$  viscosity increase causes the subducting slab in our reference free OP model to flatten in the mid-mantle. The recent two-plate, thermomechanical free subduction models of Garel *et al.* (2014) show that, with a mid-mantle viscosity jump of factor 30 and variable OP and SP ages, the wide range of slab morphologies observed on Earth can be generated. While we mostly focus on the OP mechanical properties while holding the SP properties fixed, and so a narrower parameter space than Garel *et al.* (2014), we find that our models produce at least two of the modes of deformation observed. Our free OP reference model flattens above 660 km and then stagnates, analogous to Garel *et al.* (2014) ‘horizontally deflecting’ mode, and our fixed OP subducts near-vertically with a near-stagnant trench and folds at the viscosity discontinuity, analogous to their ‘vertically folding’ mode. We find that the rate of trench rollback increases as the slab sinks through the upper mantle, and then begins to reduce once the slab feels the effect of the viscosity discontinuity (e.g. Zhong & Gurnis 1995). This reduction in rollback rate is greater for models in which the mid-mantle viscosity increase is greater (Fig. 3b). This observation of reduced rollback is important in subsequent discussions of OP stress state, and is consistent with two-plate modelling studies that parameterize the discontinuity similarly (e.g. Zhong & Gurnis 1995; Enns *et al.* 2005; Garel *et al.* 2014), and studies that treat the discontinuity as an impenetrable free/no slip boundary (e.g. Duarte *et al.* 2013; Schellart & Moresi 2013).

#### 4.1.3 Overriding plate stress state

Recent 3-D, dynamic subduction models with an OP have suggested that toroidal flow due to slab rollback is the main driver of OP extension (Duarte *et al.* 2013; Meyer & Schellart 2013; Schellart & Moresi 2013). In our 2-D models, toroidal flow is, by definition, absent. However, we still generate significant OP extensional normal stresses for models with ( $\geq 20$  MPa) and without ( $\geq 30$  MPa) a mid-mantle viscosity jump, and Earth-like mechanical and rheological parameters. Because toroidal flow is absent, our results are therefore most directly applicable to subduction segments towards the centre of very wide subduction zones where poloidal flow is likely dominant (e.g. South America, Melanesia). We observe elevated extensional stresses over a broad ( $\sim 900$  km) region, and at large distances ( $\geq 350$  km) from the plate boundary in our models. This suggests that these extensional stresses are related to basal tractions (e.g. Sleep & Toksoz 1971), as opposed to rollback induced trench suction which would be expected to occur in the region near the plate interface (e.g. Shemenda 1993).

Extensional stresses in the OP are induced by a trench directed increase in horizontal basal traction as the upwelling component of the return flow becomes horizontal below the lithosphere (e.g. Sleep & Toksoz 1971; Toksoz & Hsui 1978; Schellart & Moresi 2013). A basal traction origin is also supported by the increase in trench, ‘backarc’ distance that occurs when the mid-mantle viscosity jump is absent and the return flow cell is widened (*cf.* Figs 4a and e), and the occurrence of significant extensional stresses even when the OP is separated from the SP by mantle material (i.e. Section 3.2: ‘shallow mantle wedge’ models). Horizontal compression ( $\geq 20$  MPa) occurs near to the plate boundary, and is a result of rapid mantle wedge flow dragging the OP towards the plate interface at a rate more rapid than trench retreat (Capitanio *et al.* 2010a; Schellart & Moresi 2013; Nakakuki & Mura 2013). While this study focuses on the mechanical properties of the lithosphere, previous modelling results show that the OP stress state is strongly affected by viscos-

ity and buoyancy anomalies within the mantle wedge (Billen *et al.* 2003).

The coexistence of a compressional forearc and extensional backarc is in agreement with previous numerical modelling studies, both in 3-D (Schellart & Moresi 2013) and 2-D domains (Capitanio *et al.* 2010a; Nakakuki *et al.* 2010; Nakakuki & Mura 2013). This suggests a departure from either of the two idealized models of either slab or OP-driven trench motion, as the OP would be expected to be in pure extension or compression if the trench retreat was, respectively, purely slab or OP-driven (e.g. Jarrard 1986; Heuret *et al.* 2007; Schellart *et al.* 2007). Additionally, the OP stress regime in our reference model has a strong time dependence (e.g. Capitanio *et al.* 2010a), with a shift towards a more compressive OP once the slab has reached the mid-mantle viscosity increase (e.g. Figs 4e and g), a feature not observed in the model without a mid-mantle viscosity jump (Figs 4a and c). Slabs are more steeply dipping during the earlier, extensional phase, which is consistent with the observation that extensional backarc basins typically occur above steeply dipping slabs (Uyeda & Kanamori 1979; Lallemand & Heuret 2005). The shift, from an extensional to a compressional OP, occurs due to the reduction in the rate of trench retreat that occurs as the relatively weak slab is obstructed by the mid-mantle viscosity discontinuity (Zhong & Gurnis 1995; Christensen 1996; Čížková *et al.* 2002), which allows the tractions in the mantle wedge nose to drag the OP into the SP hinge. The amplitude of backarc extension decreases because the interaction of the slab with the viscosity discontinuity causes a change in the style of return flow from fast, localized return flow cell to more sluggish, longer wavelength return flow which does not produce the basal traction gradients required to induce significant extensional stress. Therefore, the physical nature of the phase transitions on Earth, and how they are parameterized in such geodynamic models, potentially plays a significant role in dictating OP stress state and its temporal evolution.

As observed by Capitanio *et al.* (2010a,b) and Nakakuki & Mura (2013), fixing the OP subjects it to elevated extension ( $\sim 35$  MPa) as a result of plate thinning. There is still a small region of low amplitude ( $\geq 5$  MPa) fore-arc compression in the fixed OP models (slab-flattening phase), suggesting that moderate near-trench compressional stresses, due to rapid mantle flow in the nose of the mantle wedge, may be a ubiquitous feature regardless of the OP mobility.

## 4.2 Subducting slab kinematics and overriding plate stress

Despite rollback being ‘slab driven’ in the case of free subduction, we find that the physical properties of the OP have a substantial effect on the partitioning of subduction between plate advance and rollback, and therefore slab dip (Uyeda & Kanamori 1979; Kincaid & Olson 1987; Griffiths *et al.* 1995; Christensen 1996). While our models do not include the far-field forcing that is necessary to test the hypothesis that trench rollback is controlled by the motion of the OP (e.g. Jarrard 1986; Heuret & Lallemand 2005; Heuret *et al.* 2007), previous modelling work of van Dinther *et al.* (2010) demonstrates that an externally forced OP can modify trench motion. Our discussion therefore focuses on the role that the lithospheric properties, namely viscosity, thickness and density, have in modulating the ‘free’ rate of slab rollback and the OP stress state.

### 4.2.1 Plate viscosity

Varying the lithospheric viscosity, of both the SP and the OP, exerts a strong control on both SP kinematics (Fig. 7) and OP stress (Fig. 8).

During the free sinking phase, our strong slab models have the lowest slab rollback rates ( $V_T$ ), and the steepest dips due to an increased stiffness in the bending region which resists unbending during slab descent (Conrad & Hager 1999; Enns *et al.* 2005; Di Giuseppe *et al.* 2008; Ribe 2010). The slab in the weak plate slab model has a lower dip angle during the free-sinking phase (*cf.* Figs 8b and f). This is compatible with single-plate compositional models that observe steep upper mantle dips and subsequent slab rollover or folding above the discontinuity for strong slabs (e.g. Enns *et al.* 2005; Di Giuseppe *et al.* 2008; Ribe 2010), and observations of old oceanic slabs dipping near-vertically in the western pacific subduction zones (e.g. Di Giuseppe *et al.* 2009).

As the slab tip touches the mid-mantle viscosity increase, there is a significant decrease in  $V_T$  for the slab in the weak plate model, while  $V_T$  in the strong slab model is unaffected (Fig. 7a; e.g. Zhong & Gurnis 1995; Enns *et al.* 2005). This reduction in  $V_T$  in the weak slab model causes the net OP compression to become strongly positive (Fig. 9a), giving rise to an OP dominated by compressional stresses (Fig. 8c). Our models therefore confirm that, as observed previously (Capitanio *et al.* 2010a; Nakakuki & Mura 2013; Schellart & Moresi 2013), OP compression occurs in models in which deformation and rollback is ‘slab-driven’. This contradicts the classic model of slab-driven rollback, in which solely OP plate extension accompanies rollback. The net OP convergence in the strong slab model also increases slightly during the latter stages of subduction but never becomes positive (Fig. 9a), resulting in an OP that is dominated by extensional stresses throughout subduction (Fig. 8). The lithospheric viscosity is, therefore, a key parameter in determining the OP stress state in such two-plate models. The slab-driven model predicts that an increase in OP extension is due to increased slab rollback (e.g. Elsasser 1971; Schellart 2008a). However, for the strong lithosphere model, the rollback velocity is reduced (relative to the weak plate model), while the OP becomes more extensional. This suggests that, due to the variable motion of the OP trailing edge, a simple correlation between  $V_T$  and OP deformation style may not be expected even in the case of ‘slab-driven’ rollback and deformation.

The inclusion of a stress-dependent viscosity reduces the lithospheric viscosity in localized regions, particularly in the hinge region of the SP where bending stresses are large (e.g. Billen & Hirth 2005; Enns *et al.* 2005; Stegman *et al.* 2006; Di Giuseppe *et al.* 2008). The resulting SP kinematics and OP stress regimes, for all rheologies (power law viscosity, and Byerlee plasticity), are comparable to that of the weak plate model discussed above, in that the mid-mantle viscosity increase causes a reduction in  $V_T$  which results in strong OP compression. This indicates that the strength of the SP is a key control on the OP stress regime in free OP models and that weakening the slab, either using a stress-dependent rheology or a reduced bulk viscosity, promotes OP compression.

Our simplified power law rheology gives rise to only minor viscosity reductions in mantle surrounding the slab. Therefore, we do not expect to observe an increase in plate velocity due to reduced mantle tractions, or an increase in slab dip associated with reduced hydrodynamic suction as seen in previous fixed-trench models (Tovish *et al.* 1978; Billen & Hirth 2005, 2007; Billen 2008). However, we suggest that an increase in rollback during the free-sinking phase, due to a reduced strength SP hinge, may override this dip effect in models with mobile trenches. The dominant control of the SP viscosity, over the OP viscosity, is supported by models in which only the OP viscosity is varied. Neither the subducting slab shape or the OP stress regime are strongly affected by the OP viscosity for the free OP models.

In addition to  $V_T$  and the OP stress state, the SP viscosity strongly affects the vertical slab sinking velocity ( $V_z$ ). A reduction in SP viscosity, either due to stress-dependent weakening or a reduced bulk viscosity, increases  $V_z$ . As the SP density is equivalent in these models, this increase in ( $V_z$ ) can be attributed to the decrease in hinge stiffness. For a low viscosity SP, a low hinge stiffness ( $\propto$  plate viscosity  $\times$  thickness<sup>3</sup>, for an isoviscous plate) causes a reduction in the dissipation of gravitational potential energy as the SP bends at the trench (Conrad & Hager 1999; Ribe 2010).

#### 4.2.2 Overriding plate thickness and density

The OP thickness ( $h_{op}$ ) and buoyancy ( $\Delta\rho_{op} = \rho_{op} - \rho_m$ ) both have strong effects on  $V_T$  and the OP stress regime. As observed in the dynamic two-plate models of Garel *et al.* (2014) and Sharples *et al.* (2014), and the experiments of Meyer & Schellart (2013), increasing  $h_{op}$  reduces the slab rollback velocity resulting in decreased  $V_T/V_P$  and greater dip angles. This reduced rollback is a more significant effect on the slab dip than the elevated hydrodynamic suction that, due to a larger high viscosity region (OP) above the subduction interface, tends to flatten the slab (e.g. Dvorkin *et al.* 1993). Rodríguez-González *et al.* (2012) find that slabs subducting beneath older, thicker OPs have reduced dips due to an increased hydrodynamic suction, but these models have fixed trenches and so do not take into account variation in slab rollback which has a strong effect on slab dip (e.g. Kincaid & Olson 1987; Griffiths *et al.* 1995).

Additionally, varying  $\Delta\rho_{op}$  has a strong effect on the rate of trench retreat ( $V_T$ ) with slabs with positively buoyant OPs ( $\Delta\rho_{op} = -130 \text{ kg m}^{-3}$ ) exhibiting faster rollback than those with negatively buoyant OPs ( $\Delta\rho_{op} = 130 \text{ kg m}^{-3}$ ; Fig. 14c). Increased rollback for slabs subducting beneath positively buoyant OPs, analogous to continental OPs or oceanic lithosphere with thick crust (Shemenda 1993), occurs due to the lateral hydrostatic pressure gradient ( $=\Delta\rho gh$ ) which is directed from the OP to the SP. This pressure gradient acts to push the SP backwards, thereby enhancing rollback (and reducing slab dip). This enhanced rollback is accommodated by an extensional, spreading OP (Figs 15a and c) (Figs 15a and c; e.g. Shemenda 1993). When the OP is negatively buoyant, the opposite is true, and the pressure gradient is directed towards the OP which reduces rollback and enhances OP compression. Such an increase in slab rollback, and reduction in slab dip angle, for subduction beneath a positively buoyant continental OP could potentially offset the decrease in rollback that we observe to be associated with subduction beneath a thick OP. Capitanio *et al.* (2010b) find that subduction partitioning, between rollback and plate advance, is unaffected by  $\Delta\rho_{op}$ . As mentioned previously, this is potentially due to the stiff SP core used by Capitanio *et al.* (2010a) placing a stronger constraint on SP evolution than the lateral pressure gradients induced by an OP–SP density contrast.

#### 4.2.3 Properties of fixed overriding plates

While the previous discussion has focused on subduction beneath free OPs (i.e. not attached to model sidewall), it is found that the OP mechanical properties play a stronger role in dictating slab rollback rates for models with fixed OPs. This is because rollback is forced to occur at the expense of OP thinning (e.g. Capitanio *et al.* 2010a,b), which is dictated by the OP’s tensile strength (Ribe 2001:  $\propto \eta'_{op} h_{op}$ ). Increasing OP strength, either by increasing  $h_{op}$  or  $\eta'_{op}$ , drastically reduces slab rollback which, in turn, increases the dip of the slab and

its penetrative power through the viscosity discontinuity (Griffiths *et al.* 1995; Christensen 1996; Capitanio *et al.* 2010b). The OP density,  $\Delta\rho_{op}$ , also exerts a stronger control on  $V_T$  in the fixed OP models. This is because heavy, fixed OPs resist the gravitational spreading required to facilitate rollback (Shemenda 1993), while rollback can occur via OP translation in the free OP models.

Therefore, one may expect the mechanical properties of OPs that relatively immobile (e.g. large continental OPs) to exert a stronger control on the rollback, and dip angle, of the subducting slab, relative to OPs that are more mobile (e.g. with ridge/basin proximal to the trench). As there is only a weak correlation between oceanic SP age and slab dip (Jarrard 1986; Lallemand & Heuret 2005), the variability in OP density, thickness, and in the case of a fixed OP, viscosity, potentially plays a significant role in explaining the wide range of slab rollback rates, and dip angles, observed on Earth. The slab sinking velocity is, however, independent of whether the OP is free or fixed. As pointed out previously (e.g. Conrad & Hager 1999; Capitanio *et al.* 2010a; Meyer & Schellart 2013), the suggests that the properties of the subducting slab, namely the negative buoyancy and hinge stiffness, controls vertical slab sinking.

## 5 CONCLUSIONS

We use 2-D, dynamic models of subduction with an OP to investigate the controls on the subducting slab, and stress state of the OP. In all of the models, with OPs that are both free to move and attached to the sidewall, the subducting slab rolls back. Removal of the OP elevates the slab rollback velocity to a value that is significantly faster than the SP velocity, which results in reduced slab dip angles (e.g. Yamato *et al.* 2009). In contrast, fixing the position of the trailing edge of the OP greatly reduces the rate of slab rollback, which gives to an increased slab dip angle (e.g. Capitanio *et al.* 2010a).

Despite the absence of toroidal flow, which has been shown to drive OP extension in 3-D models (e.g. Meyer & Schellart 2013; Schellart & Moresi 2013), basal tractions due to poloidal mantle return flow are sufficiently large to generate significant OP extensional stresses (>20 MPa) in our 2-D models. Simultaneously, the region nearer to the trench is under compression, due to rapid mantle wedge flow dragging the OP into the SP, at a velocity faster than the rate of rollback. Additionally, the OP stress state is strongly time dependent. As the subducting slab impinges on the high viscosity lower mantle, the slab rollback rate is reduced which, because the reduction in the velocity of the OP trailing edge is more minor, causes a shift towards stronger OP compression. It is found that the SP viscosity exerts a strong control on the OP stress state. Low viscosity subducting slabs, either due to a reduced bulk viscosity or a stress-dependent rheology, give rise to compressional OPs. Lower viscosity slabs also have elevated sinking velocities due to a reduction in the stiffness, and so bending resistance, of the SP hinge.

While the mechanical properties of solely the OP have only a minor effect on the slab sinking and SP velocities, we find that they exert a substantial control on slab rollback, and the OP stress state. Reducing the thickness of the OP gives rise to increased slab rollback rates and elevated OP stress, both compressional and extensional. Reducing the density of the OP, so that it is neutrally or positively buoyant, enhances slab rollback which results in reduced slab dips and a shift from simultaneous OP compression and extension, to solely extension. In addition, fixing the lateral edge of the OP strengthens the dependence of rollback rate, and OP stress

regime, on OP mechanical properties (e.g. Capitanio *et al.* 2010a,b). While rollback and OP deformation is driven by the negative buoyancy of the SP in such models of free-subduction, we therefore suggest that the physical properties and mobility of the OP potentially play a significant role in modulating both slab rollback and OP deformation.

## ACKNOWLEDGEMENTS

This study was partially funded by NSF grant EAR-1215720 to TWB. We thank Dave Stegman and an anonymous reviewer for constructive suggestions that significantly improved the manuscript.

## REFERENCES

- Androvičová, A., Čížková, H. & van den Berg, A.P., 2013. The effects of rheological decoupling on slab deformation in the Earth's upper mantle, *Stud. Geophys. Geod.*, **57**, 460–481.
- Becker, T.W., Faccenna, C., O'Connell, R.J. & Giardini, D., 1999. The development of slabs in the upper mantle: insights from experimental and laboratory experiments, *J. geophys. Res.*, **104**, 15 207–15 226.
- Běhouková, M. & Čížková, H., 2008. Long-wavelength character of subducted slabs in the lower mantle, *Earth planet. Sci. Lett.*, **275**, 43–53.
- Bellahsen, N., Faccenna, C. & Funiciello, F., 2005. Dynamics of subduction and plate motion in laboratory experiments: insights into the “plate tectonics” behavior of the Earth, *J. geophys. Res.*, **110**, doi:10.1029/2004JB002999.
- Billen, M.I., 2008. Modeling the dynamics of subducting slabs, *Ann. Rev. Earth Planet. Sci.*, **36**, 325–356.
- Billen, M.I. & Hirth, G., 2005. Newtonian versus non-Newtonian upper mantle viscosity: implications for subduction initiation, *Geophys. Res. Lett.*, **32**, doi:10.1029/2005GL023457.
- Billen, M.I. & Hirth, G., 2007. Rheologic controls on slab dynamics, *Geochem. Geophys. Geosyst.*, **8**, doi:10.1029/2007GC001597.
- Billen, M.I., Gurnis, M. & Simons, M., 2003. Multiscale dynamics of the Tonga-Kermadec subduction zone, *Geophys. J. Int.*, **153**, 359–388.
- Bottrill, A.D., van Hunen, J. & Allen, M.B., 2012. Insight into collision zone dynamics from topography: numerical modelling results and observations, *Sol. Earth*, **3**, 387–389.
- Butterworth, N.P., Quevedo, L., Morra, G. & Müller, R.D., 2012. Influence of overriding plate geometry and rheology on subduction, *Geochem. Geophys. Geosyst.*, **13**, doi:10.1029/2011GC003968.
- Byerlee, J.D., 1968. Brittle-ductile transition in rocks, *J. geophys. Res.*, **73**, 4741–4750.
- Capitanio, F.A., Stegman, D.R., Moresi, L. & Sharples, W., 2010a. Upper plate controls on deep subduction, trench migrations and deformations at convergent margins, *Tectonophysics*, **483**, 80–92.
- Capitanio, F.A., Zlotnik, S. & Faccenna, C., 2010b. Controls on subduction reorganization in the hellenic margin, eastern mediterranean, *Geophys. Res. Lett.*, **37**, doi:10.1029/2010GL044054.
- Capitanio, F.A., Faccenna, C., Zlotnik, S. & Stegman, D.R., 2011. Subduction dynamics and the origin of andean orogeny and the bolivian orocline, *Nature*, **480**, 83–86.
- Carlson, R.L. & Melia, P.J., 1984. Subduction hinge migration, *Tectonophysics*, **102**, 1–16.
- Chertova, M.V., Geenen, T., van den Berg, A. & Spakman, W., 2012. Using open sidewalls for modelling self-consistent lithosphere subduction dynamics, *Sol. Earth*, **3**, 313–326.
- Christensen, U., 1996. The influence of trench migration on slab penetration into the lower mantle, *Earth planet. Sci. Lett.*, **140**, 27–39.
- Čížková, H. & Bina, C., 2013. Effects of mantle and subduction-interface rheologies on slab stagnation and trench rollback, *Earth planet. Sci. Lett.*, **379**, 95–103.
- Čížková, H., van Hunen, J., van den Berg, A.P. & Vlaar, N.J., 2002. The influence of rheological weakening and yield stress on the interaction of

- slabs with the 670-km discontinuity, *Earth planet. Sci. Lett.*, **199**, 447–457.
- Čížková, H., van Hunen, J. & van den Berg, A., 2007. Stress distribution within subducting slabs and their deformation in the transition zone, *Phys. Earth planet. Inter.*, **161**, 202–214.
- Clark, S.R., Stegman, D. & Muller, R.D., 2008. Episodicity in back-arc tectonic regimes, *Phys. Earth planet. Inter.*, **171**, 265–279.
- Conrad, C. & Hager, B., 1999. Effects of plate bending and fault strength at subduction zones on plate dynamics, *J. geophys. Res.*, **104**, 17 551–17 571.
- Davies, G.F., 1995. Penetration of plates and plumes through the mantle transition zone, *Earth planet. Sci. Lett.*, **133**, 507–516.
- Di Giuseppe, E., van Hunen, J., Funiciello, F., Faccenna, C. & Giardini, D., 2008. Slab stiffness control of trench motion: insights from numerical models, *Geochem. Geophys. Geosyst.*, **9**, doi:10.1029/2007GC001776.
- Di Giuseppe, E., Faccenna, C., Funiciello, F., van Hunen, J. & Giardini, D., 2009. On the relation between trench migration, seafloor age, and the strength of the subducting lithosphere, *Lithosphere*, **1**(2), 121–128.
- Duarte, J.C., Schellart, W.P. & Cruden, A.R., 2013. Three-dimensional dynamic laboratory models of subduction with an overriding plate and variable interplate rheology, *Geophys. J. Int.*, **195**, 47–66.
- Dvorkin, J., Nur, A., Mavko, G. & Ben-Avraham, Z., 1993. Narrow subducting slabs and the origin of backarc basins, *Tectonophysics*, **227**, 63–79.
- Elsasser, W.M., 1971. Sea-floor spreading as thermal convection, *J. geophys. Res.*, **76**(5), 1101–1112.
- Enns, A., Becker, T.W. & Schmelting, H., 2005. The dynamics of subduction and trench migration for viscosity stratification, *Geophys. J. Int.*, **160**, 761–775.
- Faccenna, C., Heuret, A., Funiciello, F., Lallemand, S. & Becker, T., 2007. Predicting trench and plate motion from the dynamics of a strong slab, *Earth planet. Sci. Lett.*, **257**, 29–36.
- Forsyth, D. & Uyeda, S., 1975. On the relative importance of the driving forces of plate motion, *Geophys. J. R. astr. Soc.*, **43**, 163–200.
- Frank-Kamenetskii, D.A., 1969. *Diffusion and Heat Transfer in Chemical Kinetics*, Plenum.
- Funiciello, F., Faccenna, C., Giardini, D. & Regenauer-Lieb, K., 2003. Dynamics of retreating slabs: 2. Insights from three-dimensional laboratory experiments, *J. geophys. Res.*, **108**, doi:10.1029/2001JB000896.
- Funiciello, F., Faccenna, C., Heuret, A., Lallemand, S., Di Giuseppe, E. & Becker, T.W., 2008. Trench migration, net rotation and slabmantle coupling, *Earth planet. Sci. Lett.*, **271**, 233–240.
- Garel, F., Goes, S., Davies, D.R., Davies, J.H., Kramer, S.C. & Wilson, C.R., 2014. Interaction of subducted slabs with the mantle transition-zone: a regime diagram from 2-D thermo-mechanical models with a mobile trench and an overriding plate, *Geochem. Geophys. Geosyst.*, **15**, doi:10.1002/2014GC005257.
- Garfunkel, Z., Anderson, C.A. & Schubert, G., 1986. Mantle circulation and the lateral migration of subducted slabs, *J. geophys. Res.*, **91**, 7205–7223.
- Ghazian, R.K. & Buiter, S.J.H., 2013. A numerical investigation of continental collision styles, *Geophys. J. Int.*, **193**, 1133–1152.
- Griffiths, R.W., Hackney, R.I. & van der Hilst, R.D., 1995. A laboratory investigation of effects of trench migration on the descent of subducted slabs, *Earth planet. Sci. Lett.*, **133**, doi:10.1016/0012-821X(95)00027-A.
- Gurnis, M. & Hager, B., 1988. Controls on the structure of subducted slabs, *Nature*, **335**, 317–321.
- Han, L. & Gurnis, M., 1999. How valid are dynamic models of subduction and convection when plate motions are prescribed?, *Phys. Earth planet. Inter.*, **110**, 235–246.
- Heuret, A. & Lallemand, S., 2005. Plate motions, slab dynamics and back-arc deformation, *Phys. Earth planet. Inter.*, **149**, 31–51.
- Heuret, A., Funiciello, F., Faccenna, C. & Lallemand, S., 2007. Plate kinematics, slab shape, and back-arc stress: a comparison between laboratory models and current subduction zones, *Earth planet. Sci. Lett.*, **256**, 473–483.
- Hirth, G. & Kohlstedt, D.L., 2003. Rheology of the upper mantle and the mantle wedge: a view from the experimentalists, in *Inside the Subduction Factory*, Vol. 138, pp. 83–105, ed. Eiler, J., *Geophys. Monogr. Ser.*, AGU.
- Jarrard, R.D., 1986. Relations among subduction parameters, *Rev. Geophys.*, **24**, 217–284.
- Karato, S. & Wu, P., 1993. Rheology of the upper mantle: a synthesis, *Science*, **260**, 771–778.
- Kincaid, C. & Olson, P., 1987. An experimental study of subduction and slab migration, *J. geophys. Res.*, **92**, 13 832–13 840.
- King, S. & Hager, B., 1994. Subducted slabs and the geod. 1. numerical experiments with temperature dependent viscosity, *J. geophys. Res.*, **99**, 19 843–19 852.
- Lallemand, S. & Heuret, A., 2005. On the relationships between slab dip, back-arc stress, upper plate absolute motion, and crustal nature in subduction zones, *Geochem. Geophys. Geosyst.*, **6**(9), doi:10.1029/2005GC000917.
- Li, C., van der Hilst, R.D., Engdahl, R.E. & Burdick, S., 2008. A new global model for p wave speed variations in Earth's mantle, *Geochem. Geophys. Geosyst.*, **9**(5), doi:10.1029/2007GC001806.
- McNamara, A.K., Karato, S. & van Keeken, P.E., 2001. Localization of dislocation creep in the lower mantle: implications for the origin of seismic anisotropy, *Earth planet. Sci. Lett.*, **191**, 85–99.
- Meyer, C. & Schellart, W.P., 2013. Three-dimensional dynamic models of subducting plate-overriding plate-upper mantle interaction, *J. geophys. Res.*, **118**, 775–790.
- Molnar, P. & Atwater, T., 1978. Interarc spreading and cordilleran tectonics as alternates related to the age of subducted oceanic lithosphere, *Earth planet. Sci. Lett.*, **41**, 330–340.
- Moresi, L.N. & Gurnis, M., 1996. Constraints on the lateral strength of slabs from three-dimensional dynamic flow models, *Earth planet. Sci. Lett.*, **138**, 15–28.
- Nakakuki, T. & Mura, E., 2013. Dynamics of slab rollback and induced back-arc basin formation, *Earth planet. Sci. Lett.*, **361**, doi:10.1016/j.epsl.2012.10.031.
- Nakakuki, T., Tagawa, M. & Iwase, Y., 2010. Dynamical mechanisms controlling formation and avalanche of a stagnant slab, *Phys. Earth planet. Inter.*, **183**, 309–320.
- Quinquis, M.E.T., Buiter, S.J.H. & Ellis, S., 2011. The role of boundary conditions in numerical models of subduction zone dynamics, *Tectonophysics*, **497**, 57–70.
- Ribe, N.M., 2001. Bending and stretching of thin viscous sheets, *J. Fluid Mech.*, **433**, 135–160.
- Ribe, N.M., 2010. Bending mechanics and mode selection in free subduction: a thin-sheet analysis, *Geophys. J. Int.*, **180**, 559–576.
- Rodríguez-González, J., Negredo, A.M. & Billen, M.I., 2012. The role of the overriding plate thermal state on slab dip variability and on the occurrence of flat subduction, *Geochem. Geophys. Geosyst.*, **13**, doi:10.1029/2012GC003859.
- Schellart, W.P., 2004. Quantifying the net slab pull force as a driving mechanism for plate tectonics, *Geophys. Res. Lett.*, **31**(7), doi:10.1029/2004GL019528.
- Schellart, W.P., 2008a. Subduction zone trench migration: slab driven or overriding-plate-driven?, *Phys. Earth planet. Inter.*, **170**, 73–88.
- Schellart, W.P., 2008b. Kinematics and flow patterns in deep mantle and upper mantle subduction models: influence of the mantle depth and slab to mantle viscosity ratio, *Geochem. Geophys. Geosyst.*, **9**, doi:10.1029/2007GC001656.
- Schellart, W.P. & Moresi, L., 2013. A new driving mechanism for backarc extension and backarc shortening through slab sinking induced toroidal and poloidal mantle flow: results from dynamic subduction models with an overriding plate, *J. geophys. Res.*, **118**, doi:10.1002/jgrb.50173.
- Schellart, W.P., Freeman, J., Stegman, D.R., Moresi, L. & May, D.A., 2007. Evolution and diversity of subduction zones controlled by slab width, *Nature*, **446**, 308–311.
- Schott, B. & Schmelting, H., 1998. Delamination and detachment of a lithospheric root, *Tectonophysics*, **296**, 225–247.
- Sdrolias, M. & Müller, R.D., 2006. Controls on back-arc basin formation, *Geochem. Geophys. Geosyst.*, **7**, doi:10.1029/2005GC001090.
- Sharples, W., Jadamec, M.A., Moresi, L.N. & Capitanio, F.A., 2014. Overriding plate controls on subduction evolution, *J. geophys. Res.*, **119**, doi:10.1002/2014JB011163.

- Shemenda, A.I., 1993. Subduction of the lithosphere and back arc dynamics: insights from physical modeling, *J. geophys. Res.*, **98**, doi:10.1029/93JB01094.
- Sleep, N.H. & Toksoz, M.F., 1971. Evolution of marginal basins, *Nature*, **233**, 548–550.
- Stegman, D.R., Freeman, J., Schellart, W.P., Moresi, L. & May, D.A., 2006. Influence of trench width on subduction hinge rates in 3-d models of slab rollback, *Geochem. Geophys. Geosys.*, **7**, doi:10.1029/2005GC001056.
- Stegman, D.R., Farrington, R., Capitanio, F.A. & Schellart, W.P., 2010. A regime diagram for subduction styles from 3-d numerical models of free subduction, *Tectonophysics*, **483**, 29–45.
- Tagawa, M., Nakakuki, T., Kameyama, M. & Tajima, F., 2007a. The role of history-dependent rheology in plate boundary lubrication for generating one-sided subduction, *Pure appl. Geophys.*, **164**, 879–907.
- Tagawa, M., Nakakuki, T. & Tajima, F., 2007b. Dynamical modeling of trench retreat driven by the slab interaction with the mantle transition zone, *Earth Planets Space*, **59**, 65–74.
- Toksoz, M.F. & Hsui, A.T., 1978. Numerical studies of back-arc convection and the formation of marginal basins, *Tectonophysics*, **50**, 177–196.
- Tovich, A., Schubert, G. & Luyendyk, B.P., 1978. Mantle flow pressure and the angle of subduction: non-Newtonian corner flows, *J. geophys. Res.*, **83**, 5892–5898.
- Uyeda, S. & Kanamori, H., 1979. Back-arc opening and the mode of subduction, *J. geophys. Res.*, **84**, doi:10.1029/JB084iB03p01049.
- van Dinther, Y., Morra, G., Funiciello, F. & Faccenna, C., 2010. Role of the overriding plate in the subduction process: insights from numerical models, *Tectonophysics*, **484**, 74–86.
- van Hunen, J. & Allen, M.B., 2011. Continental collision and slab break-off: a comparison of 3-D numerical models with observations, *Earth planet. Sci. Lett.*, **302**, 27–37.
- van Hunen, J., van den Berg, A.P. & Vlaar, N.J., 2000. A thermo-mechanical model of horizontal subduction below an overriding plate, *Earth planet. Sci. Lett.*, **182**, 157–169.
- Wu, B., Conrad, C.P., Heuret, A., Lithgow-Bertelloni, C. & Lallemand, S., 2008. Reconciling strong slab pull and weak plate bending: the plate constraint on the strength of mantle slabs, *Earth planet. Sci. Lett.*, **272**, doi:10.1016/j.epsl.2008.05.009.
- Yamato, P., Husson, L., Braun, J., Loiselet, C. & Thieulot, C., 2009. Influence of surrounding plates on 3D subduction dynamics, *Geophys. Res. Lett.*, **36**, doi:10.1029/2008GL036942.
- Zhong, S., 2006. Constraints on thermochemical convection of the mantle from plume heat flux, plume excess temperature and upper mantle temperature, *J. geophys. Res.*, **111**, doi:10.1029/2005JB003972.
- Zhong, S. & Gurnis, M., 1995. Mantle convection with plates and mobile, faulted plate margins, *Science*, **267**, 838–843.